Maximum-entropy principle for static and dynamic high-field transport in semiconductors

M. Trovato[1] and L. Reggiani[2]
[1]*Dipartimento di Matematica, Università di Catania, Viale A. Doria, 95125 Catania, Italy*
[2]*Dipartimento di Ingegneria dell' Innovazione e Nanotechnology National Laboratory of CNR-INFM, Università di Lecce, Via Arnesano s/n, 73100 Lecce, Italy*

(Received 20 October 2005; revised manuscript received 25 January 2006; published 15 June 2006)

Within the maximum entropy principle we present a general theory able to provide, in a dynamical context, the macroscopic relevant variables for carrier transport under electric fields of arbitrary strength. For the macroscopic variables the linearized maximum entropy approach is developed including full-band effects within a total energy scheme. Under spatially homogeneous conditions, we construct a closed set of hydrodynamic equations for the small-signal (dynamic) response of the macroscopic variables. The coupling between the driving field and the energy dissipation is analyzed quantitatively by using an arbitrary number of moments of the distribution function. The theoretical approach is applied to *n*-Si at 300 K and is validated by comparing numerical calculations with ensemble Monte Carlo simulations and with experimental data.

DOI: 10.1103/PhysRevB.73.245209 PACS number(s): 72.10.Bg, 72.20.Ht, 52.25.Kn

I. INTRODUCTION

Recently, the formal derivation of hydrodynamic (HD) moment equations from the very microscopic dynamics of the physical system has been intensively studied using extended thermodynamics[1] and the *maximum entropy principle* (MEP).[1–10] Both of these approaches provide good insight into the origin of different terms entering the HD equations and into the approximations involved in their derivation. In particular, to include the details of a microscopic description (such as the energy band structure and scattering mechanisms) several simplifying assumptions have been introduced and different closure schemes have been implemented for the construction of self-consistent HD models.[3–11] In this context, the MEP approach emerged as a very promising method by offering a definite procedure to construct a macroequivalent distribution function[1,12–23] that determines the microstate corresponding to the given set of macroscopic variables. With this method, the microscopic state is obtained by maximizing the entropy of the system under the constraint that the macroscopic state is described by a fixed number of average quantities. We remark that by using this approach in a dynamical context[1–8,19,20] we differ from previous applications[15–18,21–23] in which the information theory is used as an extrapolation technique. The MEP, by itself, does not provide any information about the dynamic evolution of the system, but offers only a definite procedure for the construction of a sequence ofapproximations for the nonequilibrium distribution function. To obtain a dynamical description, it is necessary to know a set of evolution equations for the constraints, which include the kinetic details of the microscopic collisional processes. Thus, being the MEP distribution function known, we consider the Boltzmann equation (BE) to obtain a set of equations for the constraints that represents completely closed HD model in which all the constitutive functions are completely determined starting from their kinetic expressions. In this sense, the dynamical application of MEP will depend on both the constraints used in the maximization procedure and the determination of a system of evolution equations for these constraints which takes into account, in an explicit and accurate way, the kinetic collisional processes the carriers are subject to.[24] Only by knowing the correct dynamic evolution of the macroscopic quantities used as constraints is it possible to determine the correct dynamic evolution of the distribution function in phase space.[25]

Recently, this approach was found promising also to carry out a small-signal analysis in the homogeneous case.[8,9] Indeed, small-signal coefficients are of fundamental and applied importance for a complete description and characterization of the thermodynamic state of hot carriers in semiconductor materials and devices.[26–46] In particular, the study of the eigenvalues of the response matrix and the analysis of the time decay of the response functions provide valuable information both on the coupling processes and on the relaxation processes of the relevant macroscopic variables.[8,9,34,36–39,41,43]

The aim of this work is to develop and apply a general theory of MEP to the case of static and dynamic high field transport in semiconductor materials. In this way, the MEP is proved to sustain a rigorous kinetic theory that is complementary to other numerical techniques available in the literature[47–52] and with the advantage of offering a systematic classification of the macroscopic moments in terms of their physical properties. To this purpose, we consider as relevant variables an arbitrary number of moments of the distribution function using a linear approximation of the MEP. In this case the linearized maximum entropy approach is closely related to the Grad type moments method[1,2,6,7] and, as shown in Refs. 19 and 20, within this level of approximation it is possible to proceed by maximizing directly a quadratic expansion of the entropy to obtain equivalent results.

The theory will include full-band effects within a total energy scheme, thus obtaining a closed set of coupled differential equations for the macroscopic variables of interest. The moment equations will be generalized to a set of balance equations describing the dynamic response around the stationary state. This, enables us to calculate both the generalized response matrix and the generalized response functions of the relevant macroscopic variables for parabolic and nonparabolic band models. For particular cases of interest the

present approach recovers the results given in previous papers.[8,9,30,31,37,39,41,43]

The content of the paper is organized as follows. Section II presents the general theory. Section III develops the small signal response under space homogenous conditions. Section IV applies the total energy scheme to include a nonparabolic band structure. The case of n-type Si at 300 K is considered in Sec. V. Here a detailed comparison of present calculations with results obtained by Monte Carlo simulators and direct experiments is carried out. The overall agreement is used to validate the theoretical approach and to provide a systematic physical insight of the microscopic dynamics. Major conclusions are drawn in Sec. VI.

II. GENERAL THEORY

Below we develop an extended hydrodynamic approach within a total-energy scheme for a spatially homogenous electron system. At a kinetic level the microscopic description is governed by the BE for the single particle distribution function $\mathcal{F}(\vec{k},t)$

$$\frac{\partial \mathcal{F}}{\partial t} - \frac{e}{\hbar} E_i \frac{\partial \mathcal{F}}{\partial k_i} = Q(\mathcal{F}), \tag{1}$$

where e is the unit charge, E_i the electric field, k_i the wavevector, $\hbar$ the reduced Planck constant and

$$Q(\mathcal{F}) = \frac{V}{(2\pi)^3}\left\{ \int d\vec{k}' S(\vec{k},\vec{k}')\mathcal{F}(\vec{k}',t) - \int d\vec{k}' S(\vec{k}',\vec{k})\mathcal{F}(\vec{k},t) \right\}, \tag{2}$$

the collision integral for nondegenerate conditions, being $S(\vec{k}, \vec{k}')$ the total scattering rate for the transition $\vec{k}' \to \vec{k}$ and V the crystal volume.

Within the framework of the moment theory, to pass from the kinetic level of the BE to the extended HD level, for a general many-valley band model, we must consider the following set of generalized kinetic fields:

$$\psi_A(\vec{k}) = \{\varepsilon^m, \varepsilon^m u_{i_1}, \ldots, \varepsilon^m u_{i_1} \cdots u_{i_s}, \ldots\}, \tag{3}$$

where $\varepsilon(\vec{k})$ is a general single particle band energy dispersion of arbitrary form and u_i the carrier group velocity, being $m = 0, 1, \ldots, N$ and $s = 1, 2, \ldots, M$, with N, M integers labeling the maximum number of moments considered. With this approach, we consider the corresponding macroscopic quantities $F_A = \{F_{(m)}, F_{(m)|i_1}, \ldots, F_{(m)|i_1 \cdots i_s}, \ldots\}$, where

$$F_A = \int \psi_A(\vec{k})\mathcal{F}(\vec{k},t)d\vec{k} \tag{4}$$

and the following set of moment equations:[1,3–9]

$$\frac{\partial F_A}{\partial t} = -\frac{e}{\hbar} R_{Ai} E_i + P_A, \quad A = 1, \ldots, \mathcal{N}, \tag{5}$$

where $\mathcal{N}$ is the *fixed* number of moments used, and R_{Ai}, P_A indicate, respectively, the external field productions, and the collisional productions defined as

$$R_{Ai} = \int \frac{\partial \psi_A(\vec{k})}{\partial k_i} \mathcal{F}(\vec{k},t)d\vec{k}, \tag{6}$$

$$P_A = \int \psi_A(\vec{k}) Q(\mathcal{F}) d\vec{k}. \tag{7}$$

In particular, for $N = M = 1$ the above quantities admit a direct physical interpretation such as $F_{(0)} = n$ (numerical density), $F_{(1)} = W$ (total energy density), $F_{(0)|i} = nv_i$ (velocity flux density), $F_{(1)|i} = S_i$ (energy flux density). In general, for arbitrary values of (N, M), we obtain a system of differential equations of finite order where the flux of each equation becomes the field variable of the successive equation.[8]

With the above procedure, we obtain a system of balance equations in which there are some unknown *constitutive functions* $H_A = \{R_{Ai}, P_A\}$ that must be determined in terms of the variables F_A. Following information theory, one can determine systematically the H_A, by introducing the MEP in terms of generalized kinetic fields as in Eq. (3).[1–4,8,10,14,19,20] By using this approach, the distribution function takes the explicit form

$$\mathcal{F}_{\mathcal{N}} = \mathcal{F}_M \exp(-\Pi), \quad \Pi = \sum_{A=1}^{\mathcal{N}} \psi_A \hat{\Lambda}_A, \tag{8}$$

where $\hat{\Lambda}_A$ are the nonequilibrium part of the Lagrange multipliers[1,3,4,8,10] and $\mathcal{F}_M$ the local Maxwellian. By considering that for a band of general shape only the total average electron energy is a well defined quantity,[53] the MEP is applied within a total energy scheme.[5,8,9] Consistently with this choice, the local distribution function should be defined as $\mathcal{F}_M = \gamma \exp[-\beta\varepsilon(\vec{k})]$, where $\gamma = \gamma(n, W)$ and $\beta = \beta(W/n)$ are appropriate functions which can be determined by means of local equilibrium conditions[5,8]

$$n(t) = \int \mathcal{F}_M d\vec{k}, \quad W(t) = \int \varepsilon(\vec{k})\mathcal{F}_M d\vec{k}. \tag{9}$$

By expanding the distribution function in Eq. (8) around the maxwellian $\mathcal{F}_M$, up to a fixed order R, by means of the moments in Eq. (4) we obtain a set of nonlinear equations in the nonequilibrium quantities $\hat{\Lambda}_A$

$$F_A - F_A|_E = \int \psi_A \mathcal{F}_M \sum_{r=1}^{R} \frac{(-1)^r}{(r)!} \left(\sum_{B=1}^{\mathcal{N}} \psi_B \hat{\Lambda}_B \right)^r d\vec{k}. \tag{10}$$

By introducing in Eqs. (10) $\hat{\Lambda}_B$ in polynomials terms of the nonequilibrium variables F_B the nonlinear system can be inverted and the lagrange multipliers obtained.[1,3,4,10] In this way, having determined an analytic expression for the $\hat{\Lambda}_A$, both the distribution function $\mathcal{F}$ and the constitutive functions H_A can be estimated, up to the R order, as polynomials in the nonequilibrium variables whose coefficients depend on the local equilibrium quantities $\{n(\vec{r},t), W(\vec{r},t)\}$. In particular, to evaluate the collisional production P_A we consider in Eq. (2) the collision rate for acoustic intravalley transitions, within the elastic and equipartition approximations, and for

intervalley transitions with non-polar optical and acoustic phonons as reported in Refs. 3, 4, and 8.

III. SMALL-SIGNAL ANALYSIS

Linear-response functions around the bias point are known to play a fundamental role in the investigation of hot-carrier transport.[30,31,37–41,43] In the time domain they reflect both the dynamic and the relaxation processes inherent to the hot-carrier system. In the frequency domain they provide the ac coefficients of interest such as the usual differential mobility[28–31,37–41] the noise temperature,[43,46] the thermal conductivity,[42,44] etc.

The objective of this section is to carry out a general theory for the linear-response analysis in the framework of the moment approach. In particular, from the theory we obtain the analytical expression for the real and imaginary part of the ac generalized differential mobility for each moment of the distribution, thus generalizing existing results.[8,9,30,37–41]

A. Kinetic approach

By considering the steady state distribution function $\mathcal{F}_0(\vec{k})$ in the presence of a constant electric field $\vec{E}$, Eq. (1) becomes

$$-\frac{e}{\hbar}E_i\frac{\partial \mathcal{F}_0}{\partial k_i}=Q(\mathcal{F}_0). \tag{11}$$

By superimposing to $\vec{E}$ a small harmonic perturbation $\delta E_\beta(t)=E_\beta \exp(i\omega t)$, applied along the β direction, we analyze the linear response of the moments $\tilde{F}_A=F_A/n$.

In the framework of an extended linear-response theory, we introduce the moment generalized differential-mobility tensor $\mu'_{A\beta}(\omega)$ in terms of the response tensor $K_{A\beta}(t)$

$$\mu_{A\beta}=-e\int_0^\infty K_{A\beta}(t)\exp(-i\omega t). \tag{12}$$

In the linear approximation, the components of the tensor $\mu'_{A\beta}(\omega)$ are independent of the magnitude of the perturbing electric field. As a consequence, they can be described completely via the inherent characteristics of the unperturbed state of the system. In particular, if $\delta\vec{E}$ is parallel to $\vec{E}$, then $\mu'_{A\beta}(\omega)$ is the moment generalized longitudinal differential mobility. We recall that $\mu'_{A\beta}(\omega)$ is a complex quantity, the imaginary part being associated with the reactive contribution. Calculation of the $\mu'_{A\beta}(\omega)$ reduces to the determination of the Fourier transform of the response tensor

$$K_{A\beta}(t)=-\frac{1}{\hbar}\int\left[\int \psi_A(\vec{k}')G(\vec{k}',\vec{k},t)d\vec{k}'\right]\frac{\partial \mathcal{F}_0(\vec{k})}{\partial k_\beta}d\vec{k}, \tag{13}$$

where (being the carrier concentration uniform) the distribution function $\mathcal{F}_0(\vec{k})$ is normalized to unity and the $G(\vec{k}',\vec{k},t)$ is the evolution function [31] giving the probability for a carrier to make a transition from state $\vec{k}'$ to state $\vec{k}$ at time t, i.e., it is the Green function of the unperturbed Eq. (1) subject to the initial condition $G(\vec{k}',\vec{k},0)=\delta^3(\vec{k}'-\vec{k})$. In particular, from Eq. (13) for $t=0$ we obtain

$$K_{A\beta}(0)=\frac{1}{\hbar}\tilde{R}_{A\beta}|_0=\frac{1}{\hbar}\int\frac{\partial \psi_A(\vec{k})}{\partial k_\beta}\mathcal{F}_0(\vec{k})d\vec{k}, \tag{14}$$

where the $\tilde{R}_{A\beta}|_0$'s are the stationary values of the single-particle external field productions, along the electric field direction β, present in the moment balance Eq. (5).

The general procedure of calculating the linear response function from both, a direct MC simulation of the distribution function gradient in the $\vec{k}$, or a direct numerical resolution of the perturbed BE, has been used for more than two decades.[31,40,54] Such a kinetic approach has the obvious advantage of providing a complete microscopic picture of carriers transport in phase space. However, the calculation of both the generalized moment response functions and the generalized moment differential mobilities requires a considerable amount of CPU and the need to repeat a complete simulation each time any parameter of the microscopic model is varied.

A valuable alternative to the kinetic approach is given by the linear analysis of the moment balance equations obtained within the MEP formalism. In this way, we obtain an analytical closed model able to investigate the main features of the hot-carrier system in the time and frequency domains with the relevant advantage of providing a compressed information on the only basis of the knowledge of the microscopic interactions.

B. Hydrodynamic approach

The balance equations of the moments $\tilde{F}_A=F_A/n$ take the form

$$\frac{\partial \tilde{F}_A}{\partial t}+\frac{e}{\hbar}\tilde{R}_{Ai}E_i-\tilde{P}_A=0. \tag{15}$$

By assuming that at the initial time the carrier ensemble is perturbed by an electric field $\delta E\xi(t)$ along the direction of $\vec{E}$ [where $\xi(t)$ is an arbitrary function of time satisfying $|\xi(t)|\leq 1$], we calculate the deviations from the stationary values of the moments denoted, respectively, with $\delta\tilde{F}_A$. After linearizing Eqs. (15) around the stationary state, we obtain a system of equations which can be written as

$$\frac{d\delta\tilde{F}_\alpha(t)}{dt}=\Gamma_{\alpha\beta}\delta\tilde{F}_\beta(t)-e\,\delta E\xi(t)\Gamma_\alpha^{(E)}, \tag{16}$$

where the relaxation of the carrier ensemble to the stationary state is described by the response matrix $\Gamma_{\alpha\beta}$, and where the $-e\,\delta E\xi(t)\Gamma_\alpha^{(E)}$ are the perturbing forces.

Equation (16) has the formal solution[37]

$$\delta\tilde{\mathbf{F}}(t)=\exp(\mathbf{\Gamma}t)\,\delta\tilde{\mathbf{F}}(0)-e\,\delta E\int_0^t\mathbf{K}(s)\xi(t-s)ds, \tag{17}$$

where

$$\exp(\mathbf{\Gamma} t) = \mathbf{\Phi}\ \mathrm{diag}\{\exp(\lambda_1 t), \ldots, \exp(\lambda_{\mathcal{N}-1} t)\}\mathbf{\Phi}^{-1}, \quad (18)$$

$$\mathbf{K}(s) = \exp(\mathbf{\Gamma} s)\mathbf{\Gamma}^{(E)} \quad (19)$$

with λ_α the eigenvalues of $\Gamma_{\alpha\beta}$ and $\mathbf{\Phi}$ the matrix of its eigenvectors.

The eigenvalues λ_α can be real or complex conjugate, and they represent the generalized relaxation rates $\nu_\alpha = -\lambda_\alpha$. We remark, that an exact correspondence between these rates and the respective relaxation processes exists only in the relaxation time approximation for the collision integral in Eq. (2) and in the absence of coupling among the variables $\widetilde{F}_\alpha$.

The response functions $\mathbf{K}(t)$ are real by definition. They determine the linear response of the moments $\widetilde{F}_A$ to the action of a perturbation of the static electric field, and satisfy the causality principle $\mathbf{K}(t)=0$ if $t<0$. The initial values of the response functions as function of the static electric field can be calculated analytically using Eq. (19) for $s=0$. It is worth noting that, as it was obtained from the kinetic approach [see Eq. (14)], also in this case it is

$$K_A(0) = \Gamma_A^{(E)} = \frac{1}{\hbar}\widetilde{R}_A, \quad (20)$$

where $\widetilde{R}_A$ is the component of the external field productions along the electric field direction $\vec{E}$. Since at the initial time $t=0$ the moments are unperturbed, we assume that $\delta\widetilde{\mathbf{F}}(0)=0$ in Eq. (17) so that the small-signal analysis is described by the explicit form of the function $\xi(t)$. In particular, the linear response of the carrier ensemble to a steplike switching or to a small harmonic shape of the superimposed field are of special interest.

In the first case $\xi(t)=1$ for all $t>0$ and, using Eq. (19), with an integration of Eq. (17) one obtains the algebraic expression for the perturbation

$$\delta\widetilde{F}_\alpha(t) = -e\,\delta E\,\Gamma^{-1}_{\alpha\beta}[K_\beta(t) - \Gamma^{(E)}_\beta]. \quad (21)$$

The above relation can be used for a direct calculation of the differential response $\delta\widetilde{F}_\alpha(t)/\delta E$ to the steplike switching of the perturbing field and it is the solution of the differential equation

$$K_\alpha(t) = -\frac{1}{e\,\delta E}\frac{d\delta\widetilde{F}_\alpha(t)}{dt}. \quad (22)$$

This means that the linear response function $K_\alpha(t)$ is proportional to the time derivative of the corresponding perturbation $\delta\widetilde{F}_\alpha(t)$ and that to the extreme position of $\delta\widetilde{F}_\alpha$ at time $\bar{t}$ it corresponds $K_\alpha(\bar{t})=0$, that represents the same relaxation phenomenon. Analogously, by a further differentiation of Eq. (22) we obtain

$$\frac{dK_\alpha(t)}{dt} = -\frac{1}{e\,\delta E}\frac{d^2\delta\widetilde{F}_\alpha(t)}{dt^2} \quad (23)$$

and we observe that one flex point of the perturbation $\delta\widetilde{F}_\alpha$ at time t' can be associated with an extreme position of the corresponding response function $K_\alpha(t')$.

In the second case of a small harmonic perturbation $\xi(t)=\exp(i\omega t)$, we observe that at long times the upper limit in the integral of Eq. (17) can be replaced by infinity and thus we obtain a perturbation of the single-carrier moments which is also harmonic $\delta\widetilde{\mathbf{F}}(t)=\delta\widetilde{\mathbf{F}}(\omega)\exp(i\omega t)$ where

$$\delta\widetilde{F}_\alpha(\omega) = \mu'_\alpha(\omega)\,\delta E, \qquad \text{with } \mu'_\alpha(\omega) = -e\int_0^\infty K_\alpha(s)\exp(-i\omega s)ds. \quad (24)$$

By using Eq. (19), a cyclic integration by parts transforms Eq. (24) in the algebraic relation

$$\mu'_\alpha(\omega) = \sum_{r=0}^{N}\frac{-e}{(i\omega)^{r+1}}\Gamma^r_{\alpha\beta}\Gamma^{(E)}_\beta + \frac{1}{(i\omega)^{N+1}}\Gamma^{N+1}_{\alpha\beta}\mu'_\beta(\omega) \quad (25)$$

with $N=0,1,\ldots,S$, being S an arbitrary integer number. In particular, for $S=0$ we obtain

$$\mu'_\alpha(\omega) = e[\Gamma_{\alpha\beta} - i\omega\delta_{\alpha\beta}]^{-1}\Gamma^{(E)}_\beta. \quad (26)$$

By considering the real and imaginary parts separately, we have $\mu'_\alpha(\omega)=X_\alpha(\omega)+iY_\alpha(\omega)$, and by using Eq. (26)) we obtain

$$X_\alpha(\omega) = e\Gamma_{\alpha\beta}[\Gamma^2_{\beta\gamma} + \omega^2\delta_{\beta\gamma}]^{-1}\Gamma^{(E)}_\gamma, \quad (27)$$

$$Y_\alpha(\omega) = e\omega[\Gamma^2_{\alpha\gamma} + \omega^2\delta_{\alpha\gamma}]^{-1}\Gamma^{(E)}_\gamma. \quad (28)$$

It is worth noting, that in the low frequency limit the real parts $X_\alpha(\omega)$ of the ac generalized differential mobility tend to the corresponding dc values of the generalized differential mobility

$$\lim_{\omega\to 0} X_\alpha(\omega) = X_\alpha(0) = \left[\frac{d\widetilde{F}_\alpha}{dE}\right]_{\mathrm{dc}}. \quad (29)$$

In particular, for vanishing values of ω it is

$$X_\alpha(\omega) \approx X_\alpha(0) + \frac{1}{2}\left[\frac{d^2X_\alpha}{d\omega^2}\right]_0\omega^2, \quad Y_\alpha(\omega) \approx \left[\frac{dY_\alpha}{d\omega}\right]_0\omega, \quad (30)$$

where from Eqs. (24) and Eqs. (27), (28) we obtain the general relations

$$X_\alpha(0) = -e\int_0^\infty K_\alpha(s)ds = e\Gamma^{-1}_{\alpha\beta}\Gamma^{(E)}_\beta, \quad (31)$$

$$\left[\frac{dY_\alpha}{d\omega}\right]_0 = e\int_0^\infty sK_\alpha(s)ds = e(\Gamma^{-1}_{\alpha\beta})^2\Gamma^{(E)}_\beta, \quad (32)$$

$$\left[\frac{d^2X_\alpha}{d\omega^2}\right]_0 = e\int_0^\infty s^2K_\alpha(s)ds = -2e(\Gamma^{-1}_{\alpha\beta})^3\Gamma^{(E)}_\beta. \quad (33)$$

Analogously, in the high frequency limits, by using Eq. (25) (being N arbitrarily large) and Eqs. (27), (28)) we obtain the asymptotic relations

$$X_\alpha(\omega) \approx \frac{e}{\omega^2}\Gamma_{\alpha\beta}\Gamma_\beta^{(E)} = \frac{e}{\omega^2}\left[\frac{dK_\alpha}{dt}\right]_{0^+}, \tag{34}$$

$$Y_\alpha(\omega) \approx \frac{e}{\omega}\Gamma_\alpha^{(E)} = \frac{e}{\omega}K_\alpha(0). \tag{35}$$

Since $X_\alpha(\omega)$ is even in ω and $Y_\alpha(\omega)$ is odd in ω, by considering the inverse Fourier transform of Eq. (24) and using Eqs. (27), (28), (31)), the integrals of the functions X_α and Y_α/ω give

$$\int_0^\infty X_\alpha d\omega = -\frac{\pi}{2}e\Gamma_\alpha^{(E)} = -\frac{\pi}{2}eK_\alpha(0), \tag{36}$$

$$\int_0^\infty \frac{1}{\omega}Y_\alpha d\omega = -\frac{\pi}{2}e\Gamma^{-1}_{\alpha\beta}\Gamma_\beta^{(E)} = -\frac{\pi}{2}X_\alpha(0), \tag{37}$$

Analogously, by considering the integrals of the functions $[\omega Y_\alpha - e\Gamma_\alpha^{(E)}]$ and $[\omega^2 X_\alpha - e\Gamma_{\alpha\beta}\Gamma_\beta^{(E)}]$, and by using Eqs. (27), (28) we obtain

$$\int_0^\infty [\omega Y_\alpha - eK_\alpha(0)]d\omega = \frac{\pi}{2}e\Gamma_{\alpha\beta}\Gamma_\beta^{(E)} = \frac{\pi}{2}e\left[\frac{dK_\alpha}{dt}\right]_{0^+}, \tag{38}$$

$$\int_0^\infty \left[\omega^2 X_\alpha - e\left(\frac{dK_\alpha}{dt}\right)_{0^+}\right]d\omega = \frac{\pi}{2}e\Gamma^2_{\alpha\beta}\Gamma_\beta^{(E)} = \frac{\pi}{2}e\left[\frac{d^2K_\alpha}{dt^2}\right]_{0^+}, \tag{39}$$

It is worth noting that all the previous relations in Eqs. (17)–(39) are the natural generalization of the results reported in Refs. 8, 30, 37–39, and 41. We remark that, some limiting properties of the real and imaginary part of the ac generalized differential mobility μ'_α are easily extracted from Eqs. (29)–(39). Accordingly, from Eq. (29) we obtain that $X_\alpha(\omega)$ tends to the corresponding dc differential mobility $d\widetilde{F}_\alpha/dE$ when $\omega \to 0$, while from Eq. (34) $X_\alpha(\omega) \to 0$ for $\omega \to \infty$. Analogously from Eq. (30) and Eq. (35) $Y_\alpha(\omega)$ tends to zero when ω tends to zero or infinity.

From what reported above, we conclude that the advantages of the approach proposed here are the following: (i) The formulation of the ac and dc theory is carried out as at a kinetic level, and can be performed using an energy dispersion of general form (full-band approach). (ii) From the explicit determination of the response matrix $\Gamma_{\alpha\beta}$ and the vector $\Gamma_\alpha^{(E)}$, we can construct an algebraic (in place of an integral) formulation of the theory. (iii) As far as the closure relations H_A are concerned, also the small signal coefficients $\Gamma_{\alpha\beta}$, $\Gamma_\alpha^{(E)}$, $K_\alpha(t)$, $X_\alpha(\omega)$, and $Y_\alpha(\omega)$ are consistently obtained as function of both the different moments and the order of the expansion that are used to determine the distribution functions $\mathcal{F}$. In the following sections we will consider an application of the MEP in a linear context.

IV. APPLICATION OF THE TOTAL ENERGY SCHEME

We consider a total-energy scheme to describe the full complexity of the band in terms of a single particle with an effective mass function of its average total energy $\widetilde{W}$.[5,8,9] In this framework, the effective mass becomes a new constitutive function which should be independently determined from the fitting of experiments and/or from MC calculations of the bulk material.[5] The advantages of the total-energy scheme are that (i) all the constitutive relations are obtained in analytic form and (ii) the same set of balance equations describe the transport properties of the carrier ensemble for both the parabolic (when m^* is constant) and full-band cases [when $m^* = m^*(\widetilde{W})$]. The present extended HD theory does not need other adjustable parameters but the knowledge of the elementary microscopic interactions as for the kinetic theory.

A. Linear expansion with an arbitrary number of moments

The general formulation of the MEP in a *linear* context, and the construction of self-consistent closure relations with an arbitrary number of moments, was developed in Ref. 8. With this approach, the unique independent average quantities are the traceless part $F_{(p)|\langle i_1\cdots i_s\rangle}$ of the tensor $F_{(p)|i_1\cdots i_s}$. In particular, for problems with axial symmetry we can take $E_i=\{E,0,0\}$, so that only the independent components

$$F_{(p)|\langle s\rangle} = F_{(p)|\langle \underbrace{1\cdots 1}_{s \text{ times}}\rangle}$$

are of concern, where the angular brackets indicate the deviatoric[1] part of the tensor of rank s. According to this choice we obtain: for $s=0$ the scalar moments $F_{(p)}$, for $s=1$ the vectorial moments of components $F_{(p)|i}=\{F_{(p)|1},0,0\}$ and, for $s>1$ the traceless tensorial moment of rank s of which the unique independent component is $F_{(p)|\langle s\rangle}=F_{(p)|\langle 1\cdots 1\rangle}$. By considering the single carrier quantities $\widetilde{F}_A = \{\widetilde{F}_{(q)}, \widetilde{F}_{(p)|1}, \ldots, \widetilde{F}_{(p)|\langle s\rangle}\}$ the corresponding balance equations under homogeneous conditions read

$$\frac{\partial \widetilde{F}_{(q)}}{\partial t} = -eEq\widetilde{F}_{(q-1)|1} - \widetilde{P}_q^{(0)} - \sum_{l=2}^{N}\alpha_{ql}^{(0)}\widetilde{\Delta}_{(l)} \quad \text{for } q=1,\ldots,N,$$

$$\frac{\partial \widetilde{F}_{(p)|1}}{\partial t} = -eE\left\{p\widetilde{F}_{(p-1)|\langle 2\rangle} + \frac{1}{m^*}\frac{2p+3}{3}\widetilde{F}_{(p)}\right\} - \sum_{l=0}^{N}\alpha_{pl}^{(1)}\widetilde{F}_{(l)|1},$$

$$\vdots \qquad \vdots \qquad \vdots$$

$$\frac{\partial \widetilde{F}_{(p)|\langle s\rangle}}{\partial t} = -eE\left\{p\widetilde{F}_{(p-1)|\langle s+1\rangle} + \frac{1}{m^*}\frac{s^2}{2s-1}\left[\frac{2(p+s)+1}{2s+1}\right]\widetilde{F}_{(p)|\langle s-1\rangle}\right\} - \sum_{l=0}^{N}\alpha_{pl}^{(s)}\widetilde{F}_{(l)|\langle s\rangle}, \tag{40}$$

with $p=0,1,\ldots,N$ and $s=2,\ldots,M$.

The quantities $\widetilde{\Delta}_{(l)}$ represent the nonequilibrium parts of the scalar moments $\widetilde{F}_{(l)}$, where

$$\widetilde{F}_{(l)}|_E = \frac{(2l+1)!!}{3^l}\widetilde{W}^l, \quad \widetilde{\Delta}_{(l)} = \widetilde{F}_{(l)} - \widetilde{F}_{(l)}|_E. \tag{41}$$

In the linear approximation $\widetilde{F}_{(p)|\langle M+1\rangle}=0$ and the closure relations for the quantities $\{\widetilde{P}_p^{(0)}, \alpha_{pl}^{(0)}, \alpha_{ql}^{(s)}\}$ are explicitly reported in Ref. 8.

By considering the small signal theory and using Eq. (14), for the initial value of the response functions we obtain the analytic expression

$$K_{(p)|\langle s\rangle}(0) = p\widetilde{F}_{(p-1)|\langle s+1\rangle} + \frac{s^2}{2s-1}\left[\frac{2(p+s)+1}{2s+1}\right]\frac{1}{m^*}\widetilde{F}_{(p)|\langle s-1\rangle}. \tag{42}$$

We remark that for the quantities which admit a direct physical interpretation $\{\widetilde{W}=\widetilde{F}_{(1)}, v=\widetilde{F}_{(0)|1}, \widetilde{S}=\widetilde{F}_{(1)|1}\}$, it is

$$K_{\widetilde{w}}(0) = v, \quad K_v(0) = \frac{1}{m^*(\widetilde{w})}, \quad K_{\widetilde{s}}(0) = \widetilde{F}_{(0)|\langle 2\rangle} + \frac{5}{3}\frac{\widetilde{W}}{m^*(\widetilde{w})}, \tag{43}$$

where $\{v, 1/m^*\}$ are the standard response functions of moments $\{\widetilde{W}, v\}$ evaluated at $t=0$.[30,39] Analogously, it can be shown that the initial value of the response functions for the moments $\widetilde{\Delta}_{(l)}$ are expressed in terms of the quantity

$$K_{\widetilde{\Delta}_{(l)}}(0) = l\left[\widetilde{F}_{(l-1)|1} - \frac{(2l+1)!!}{3^l}\widetilde{W}^{l-1}\widetilde{F}_{(0)|1}\right], \tag{44}$$

with $l=2,\ldots,N$.

B. Time evolution of perturbations

Under stationary conditions, Eqs. (40) constitute a system of algebraic equations which numerical solution allows us to determine the moments as a function of the electric field E. By considering the time evolution of a small perturbation around the stationary state of the moments $\widetilde{F}_\alpha$, the system of Eq. (16) will be expressed in terms of the $N+(N+1)M$ quantities

$$\delta\widetilde{F}_\alpha(t) = \{\delta\widetilde{F}_{(q)}, \delta\widetilde{F}_{(p)|1}, \delta\widetilde{F}_{(p)|\langle 2\rangle}, \ldots, \delta\widetilde{F}_{(p)|\langle s\rangle}, \ldots, \delta\widetilde{F}_{(p)|\langle M\rangle}\}^T \tag{45}$$

with $q=1,\ldots,N$, $p=0,\ldots,N$.

Analogously, the vector $\Gamma_\alpha^{(E)}$ of the perturbing forces

$$\Gamma_\alpha^{(E)} = \{\Gamma_{(q)}^{(E)}, \Gamma_{(p)|1}^{(E)}, \Gamma_{(p)|\langle 2\rangle}^{(E)}, \ldots, \Gamma_{(p)|\langle s\rangle}^{(E)}, \ldots, \Gamma_{(p)|\langle M\rangle}^{(E)}\}^T, \tag{46}$$

and the asymmetric $[N+(N+1)M]\times[N+(N+1)M]$ response matrix $\Gamma_{\alpha\beta}$ given by

$$\Gamma_{\alpha\beta} = \begin{bmatrix}
\boldsymbol{\Gamma}_w^{(0)} & \mathbf{A}^{(0)} & \mathbf{B}^{(0)} & 0 & 0 & 0 & 0 & \cdots & 0 & 0 & 0 \\
\boldsymbol{\Gamma}_w^{(1)} & \mathbf{C}^{(1)} & \mathbf{A}^{(1)} & \mathbf{B}^{(1)} & 0 & 0 & 0 & \cdots & 0 & 0 & 0 \\
\boldsymbol{\Gamma}^{(2)} & 0 & \mathbf{C}^{(2)} & \mathbf{A}^{(2)} & \mathbf{B}^{(2)} & 0 & 0 & \cdots & 0 & 0 & 0 \\
\boldsymbol{\Gamma}_w^{(3)} & 0 & 0 & \mathbf{C}^{(3)} & \mathbf{A}^{(3)} & \mathbf{B}^{(3)} & 0 & \cdots & 0 & 0 & 0 \\
\boldsymbol{\Gamma}_w^{(4)} & 0 & 0 & 0 & \mathbf{C}^{(4)} & \mathbf{A}^{(4)} & \mathbf{B}^{(4)} & \cdots & 0 & 0 & 0 \\
\boldsymbol{\Gamma}_w^{(5)} & 0 & 0 & 0 & 0 & \mathbf{C}^{(5)} & \mathbf{A}^{(5)} & \cdots & 0 & 0 & 0 \\
\vdots & \vdots & \vdots & \vdots & \vdots & \vdots & \vdots & \cdots & \vdots & \vdots & \vdots \\
\boldsymbol{\Gamma}_w^{(M-1)} & 0 & 0 & 0 & 0 & 0 & 0 & \cdots & \mathbf{C}^{(M-1)} & \mathbf{A}^{(M-1)} & \mathbf{B}^{(M-1)} \\
\boldsymbol{\Gamma}_w^{(M)} & 0 & 0 & 0 & 0 & 0 & 0 & \cdots & 0 & \mathbf{C}^{(M)} & \mathbf{A}^{(M)}
\end{bmatrix}, \tag{47}$$

where all the components $\Gamma_\alpha^{(E)}$ of the vector reported in Eq. (46) are explicit functions of moments $\widetilde{F}_{(p)|\langle s\rangle}$, as reported in the Appendix.

Analogously, all the elements $\boldsymbol{\Gamma}_w^{(s)}$ of the first column of the matrix in Eq. (47) are vectors that can be expressed by introducing the chord mobility generalized moments $\mu_{(p)|\langle s\rangle} = \widetilde{F}_{(p)|\langle s\rangle}/E$ and the differential mobility generalized moments $\mu'_{(p)|\langle s\rangle} = d\widetilde{F}_{(p)|\langle s\rangle}/dE$, and the quantities $\{\mathbf{A}^{(s)}, \mathbf{B}^{(r)}, \mathbf{C}^{(n)}\}$ are submatrices explicitly calculated in terms of the coefficients $\alpha_{ql}^{(s)}$ and of the electric field (see the Appendix).

With this approach, from the analytic knowledge of the coefficients $\{\alpha_{qr}^{(s)}\}$ and from the numerical calculation of the quantities $\{\mu_{(p)|\langle s\rangle}, \mu'_{(p)|\langle s\rangle}\}$ all the elements of the matrix $\Gamma_{\alpha\beta}$ can be explicitly evaluated starting from the stationary values of the system. Analogously, the evolution of the vectorial response function $\mathbf{K}(t)$ will be expressed in terms of its $N+(N+1)M$ components for the perturbation of the moments $\widetilde{F}_\alpha$

$$K_\alpha(t) = \{K_{(q)}, K_{(p)|1}, K_{(p)|\langle 2\rangle}, \ldots, K_{(p)|\langle s\rangle}, \ldots, K_{(p)|\langle M\rangle}\}^T. \tag{48}$$

In particular, for the quantities which admit a direct physical interpretation $\{\widetilde{W}=\widetilde{F}_{(1)}, v=\widetilde{F}_{(0)|1}, \widetilde{S}=\widetilde{F}_{(1)|1}\}$, we have the

response functions $\{K_{\tilde{W}}=K_{(1)},\ K_v=K_{(0)|1},\ K_{\tilde{S}}=K_{(1)|1}\}$ obtained, respectively, for the fluctuations of mean energy, velocity and energy flux, while the remaining components of $\mathbf{K}(t)$ refer to the perturbation of other moments.

V. NUMERICAL RESULTS FOR N-SILICON

Below we apply the theory developed above to the relevant case of *n*-Si. To this purpose we consider an electric field applied along the ⟨111⟩ crystallographic axes, so that we keep the axial symmetry, and we account for full-band effects by introducing an effective mass function of the electron average total energy.[5] For the collisional processes, scattering with phonons of *f* and *g* type are considered with six possible transitions $(g_1,g_2,g_3,f_1,f_2,f_3)$. The HD calculations are performed using the physical scattering parameters in Ref. 55 and 56. MC simulations have been obtained from a full-band model[57] and an analytic nonparabolic band model.[56] For the differential mobility μ_v' as a function of electric field, we report also some experimental data obtained both in the low frequency limit[58] and at a high frequency of 123.3 GHz (Ref. 28) for *n*-Si samples oriented along the ⟨111⟩ crystallographic direction.

A. Stationary conditions

To obtain the stationary value of the moments $\tilde{F}_{(p)|\langle s\rangle}$ as a function of the electric field, the balance equations (40) are solved numerically by the Runge-Kutta procedure for stiff problems.[59]

Figure 1 reports the HD values for the moments $\tilde{F}_{(0)|\langle s\rangle}=\{v,\tilde{F}_{(0)|\langle 2\rangle},\tilde{F}_{(0)|\langle 3\rangle},\tilde{F}_{(0)|\langle 4\rangle},\tilde{F}_{(0)|\langle 5\rangle}\}$, $\tilde{F}_{(1)|\langle s\rangle}=\{\tilde{W},\tilde{S},\tilde{F}_{(1)|\langle 2\rangle},\tilde{F}_{(1)|\langle 3\rangle},\tilde{F}_{(1)|\langle 4\rangle},\tilde{F}_{(1)|\langle 5\rangle}\}$, and $\tilde{F}_{(2)|\langle s\rangle}=\{\tilde{F}_{(2)},\tilde{F}_{(2)|1},\tilde{F}_{(2)|\langle 2\rangle},\tilde{F}_{(2)|\langle 3\rangle},\tilde{F}_{(2)|\langle 4\rangle},\tilde{F}_{(2)|\langle 5\rangle}\}$ as a function of the electric field, calculated for $N=2$ and $M=5$, both in the parabolic and full-band case. For the velocity, energy, and energy flux we report the MC values of full-band simulations[57] (open circles) and analytic nonparabolic-band simulations[56] (crosses); for the velocity we report also the experimental data, obtained with the microwave time-of-flight (MTOF) technique,[32,58] and available for field strengths up to 130 KV/cm. The dependence upon the electric field of the moments is traced back to the relation between the average value of $F_{(p)|\langle i_1\cdots i_s\rangle}$ and its kinetic counterpart $\varepsilon^p u_{\langle i_1}\cdots u_{i_s\rangle}$, by recalling that the index *p* is associated with the isotropic part of the tensor $F_{(p)|\langle s\rangle}$ with the index *s* indicating the deviatoric part described by the angular brackets. For fixed values of the index *p*, and by considering different values of the deviatoric part *s*, the moments show an analogous behavior for high field values, both in the parabolic and in the full-band case. In particular, for $p=0$ all moments $F_{(0)|\langle s\rangle}$ (starting from velocity $v=F_{(0)|1}$ and for increasing values of *s*) exhibit an initial increase and then tend to saturate at the highest electric fields where the dc differential mobility vanishes. By contrast, for $p\geq 1$ all moments $F_{(p)|\langle s\rangle}$ exhibit an initial increase, but they do not saturate at high field values. In particular, at high fields, if we consider increasing values of the index *p*, then the slope (i.e., the dc differential mobility) of all curves is found to increases correspondingly. To provide a physical interpretation of the curves reported in Fig. 1, it is useful to analyze the different contributions that can be associated with the separate action of the electric field and of the scattering mechanisms. As a general trend, all the moments start increasing with increasing field because of the induced drift which breaks the time-space symmetry. For intermediate and high values of the electric field, due to the higher absorbed power and the energy dependence of the scattering mechanisms, the driving field couples with the scattering processes and we assist to an increase of the scattering efficiency. Such an increase is known to be responsible for the dissipation of the

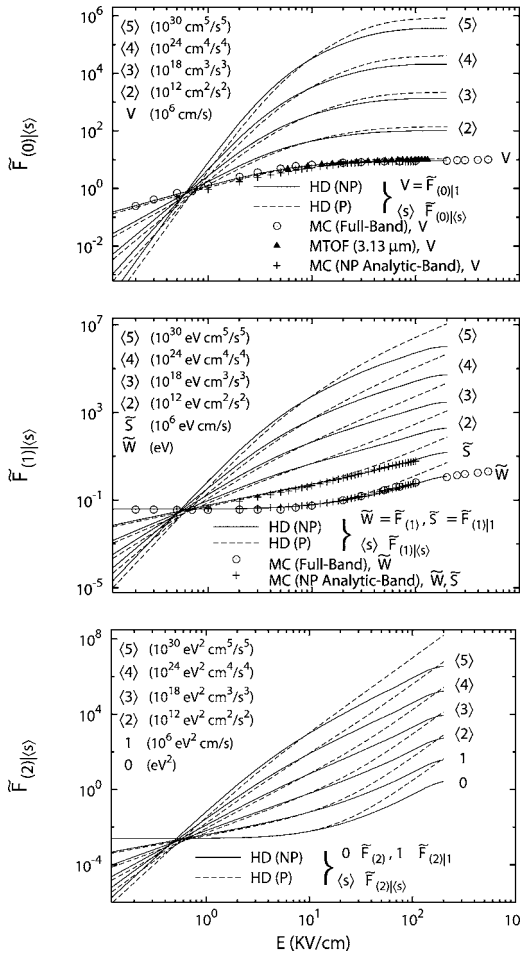

FIG. 1. Values for the moments $\tilde{F}_{(0)|\langle s\rangle}=\{v,\tilde{F}_{(0)|\langle 2\rangle},\tilde{F}_{(0)|\langle 3\rangle},\tilde{F}_{(0)|\langle 4\rangle},\tilde{F}_{(0)|\langle 5\rangle}\}$, $\tilde{F}_{(1)|\langle s\rangle}=\{\tilde{W},\tilde{S},\tilde{F}_{(1)|\langle 2\rangle},\tilde{F}_{(1)|\langle 3\rangle},\tilde{F}_{(1)|\langle 4\rangle},\tilde{F}_{(1)|\langle 5\rangle}\}$, and $\tilde{F}_{(2)|\langle s\rangle}=\{\tilde{F}_{(2)},\tilde{F}_{(2)|1},\tilde{F}_{(2)|\langle 2\rangle},\tilde{F}_{(2)|\langle 3\rangle},\tilde{F}_{(2)|\langle 4\rangle},\tilde{F}_{(2)|\langle 5\rangle}\}$ vs electric field for electrons in Si at $T_0=300$ K. Lines refer to present parabolic (dashed lines) and nonparabolic (solid lines) HD calculations with $N=2$, $M=5$. Open circles refer to full-band MC simulations (Ref. 57) performed along ⟨111⟩ crystallographic directions. Crosses refer to analytical nonparabolic band MC simulations (Ref. 56) performed along the ⟨111⟩ crystallographic direction. For the drift velocity we report also the experimental data (Refs. 32 and 58) obtained with the microwave time-of-flight technique (MTOF) along the ⟨111⟩ crystallographic direction.

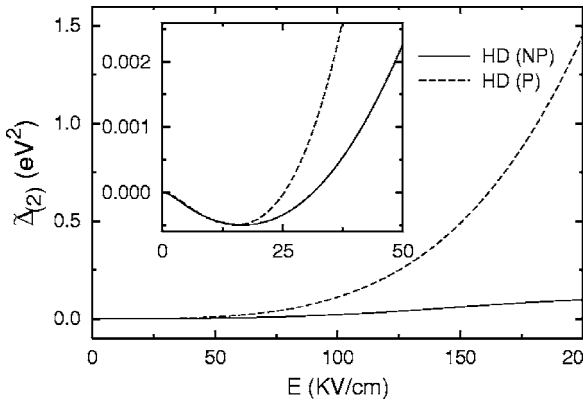

FIG. 2. $\tilde{\Delta}_{(2)}$ is the nonequilibrium part of scalar moment $\tilde{F}_{(2)}$ vs electric field for electrons in Si in the case of parabolic (P) and nonparabolic (NP) band models at $T_0=300$ K.

energy and momentum gained by charge carriers from the field. In particular, the behavior of moments $F_{(p)|\langle s\rangle}$ (for different values of indices p and s) is due essentially to the combined action of the external field which accelerates carriers in the direction of its application and of the scattering mechanisms which dissipate energy and distribute momentum in different directions. Furthermore, the applied field acts mainly on the isotropic part of the moments while the scattering mechanisms act mainly on the deviatoric part of the moments. Indeed, at high fields and for increasing values of the index p, all moments increase faster because of the reduced efficiency of scattering to dissipate the excess energy gained by the field. By contrast, for increasing values of the deviatoric part s, all moments increase slower with increasing fields because of the enhanced efficiency of scattering to dissipate through randomization the momentum gained by the field. We have verified that the HD results exhibit small variations when changing the number of moments used[8] both in the parabolic and full-band case. The energy dependence of the effective mass obtained by fitting the velocity-field curve reproduces with good accuracy the MC data of energy and energy flux, thus validating the present HD approach.

Figure 2 reports the contribution of the nonequilibrium part $\tilde{\Delta}_{(2)}$ of the scalar moment $\tilde{F}_{(2)}$. Here, $\tilde{\Delta}_{(2)}$ initially exhibits a small negative part (with a corresponding small negative dc differential mobility). Then, at increasing fields it increases monotonously both in the parabolic and full-band model. We also note that the net effect of nonparabolicity is to reduce systematically the increase of all moments with field. Such a reduction is found to be more effective for higher moments as expected. From a microscopic point of view these general behaviors are understood by the fact that scattering processes increase their efficiency at increasing carrier energy thus making their coupling with field more pronounced.

To interpret the small-signal coefficients under ac conditions, we have calculated the eigenvalues of the response matrix $\Gamma_{\alpha\beta}$ as a function of the electric field. These calculations are presented in the next section.

B. Linear analysis: Eigenvalue spectrum

In general the eigenvalues of the response matrix $\Gamma_{\alpha\beta}$ are complex quantities with the imaginary part indicating the presence of some kind of deterministic relaxation in the system that can be attributed to a streaming character of the distribution function. The extreme case of a vanishing value of the real part is well know as the condition of an ideal streaming motion regime.[33,34,36] Here, the carrier is accelerated by the field up to the energy of the optical phonon. Then, by emitting an optical phonon, it is scattered back to the bottom of the band and the cycle starts again. In our case, however, we are far from this ideal regime. Indeed, for Si at $T_0=300$ K carriers undergo other scattering events in addition to that of optical phonon emission and, therefore, the streaming-motion regime is far from being fully achieved. By using an increasing number of moments, also the number of coupled eigenvalues increases and the regions with complex eigenvalues extend significantly towards higher fields. At these fields, the process of energy and momentum dissipation becomes so strong that, to describe the part of streaming present in the system, it becomes necessary to consider many moments. When the electric field is increased further, some eigenvalues again become real quantities. At these highest fields, thermalization of the carrier system occurs at energies well above the value of optical phonons. As a consequence, no streaming is maintained anymore and transport takes a nearly full chaotic character (diffusive regime).

The moments $\tilde{F}_{(p)|\langle s\rangle}$ are characterized by the indices $p=0,1,\ldots,N$ and $s=0,1,\ldots,M$. Therefore, to interpret the eigenvalues spectrum obtained from an increasing number of moments we proceed gradually by fixing one of the two quantities (N,M) and varying the other. Anyway, the spectrum behavior becomes sufficiently intricate and in the case of complex values we represent with continuous lines the real part $-\lambda_R$ and with dashed lines the imaginary part $-\lambda_I$ of the eigenvalues of $\Gamma_{\alpha\beta}$.

Figure 3 (left part) reports the generalized relaxation rates $\nu_\alpha=-\lambda_\alpha$ obtained using only an increasing number of scalar and vectorial moments (i.e., by taking as maximum tensorial order $M=1$ with different values of the isotropic part $N=2,3,5$) in the nonparabolic band model. As a general trend, with increasing field all the vectorial rates increase because of the increase with energy of the scattering probabilities. By contrast, at the highest fields all scalar rates decrease since energy relaxation rates decrease at increasing electric fields. Numerical results show different regions, which correspond to the different character of the eigenvalues. For small and intermediate values of the electric field, there are some couples of complex conjugate eigenvalues due to the strong coupling between scalar and vectorial moments. In particular, the velocity and energy relaxation rates are coupled by the electric field practically for all the values of N with an extension of the coupling region up to about 120 KV/cm for $N=5$ in the nonparabolic case and with an imaginary part $-\lambda_I$ comparable with the real part $-\lambda_R$ in a large part of this region. When analyzing the results of Fig. 3, we see also that the width of the region with complex values and the number of coupled eigenvalues depend on the increasing number of

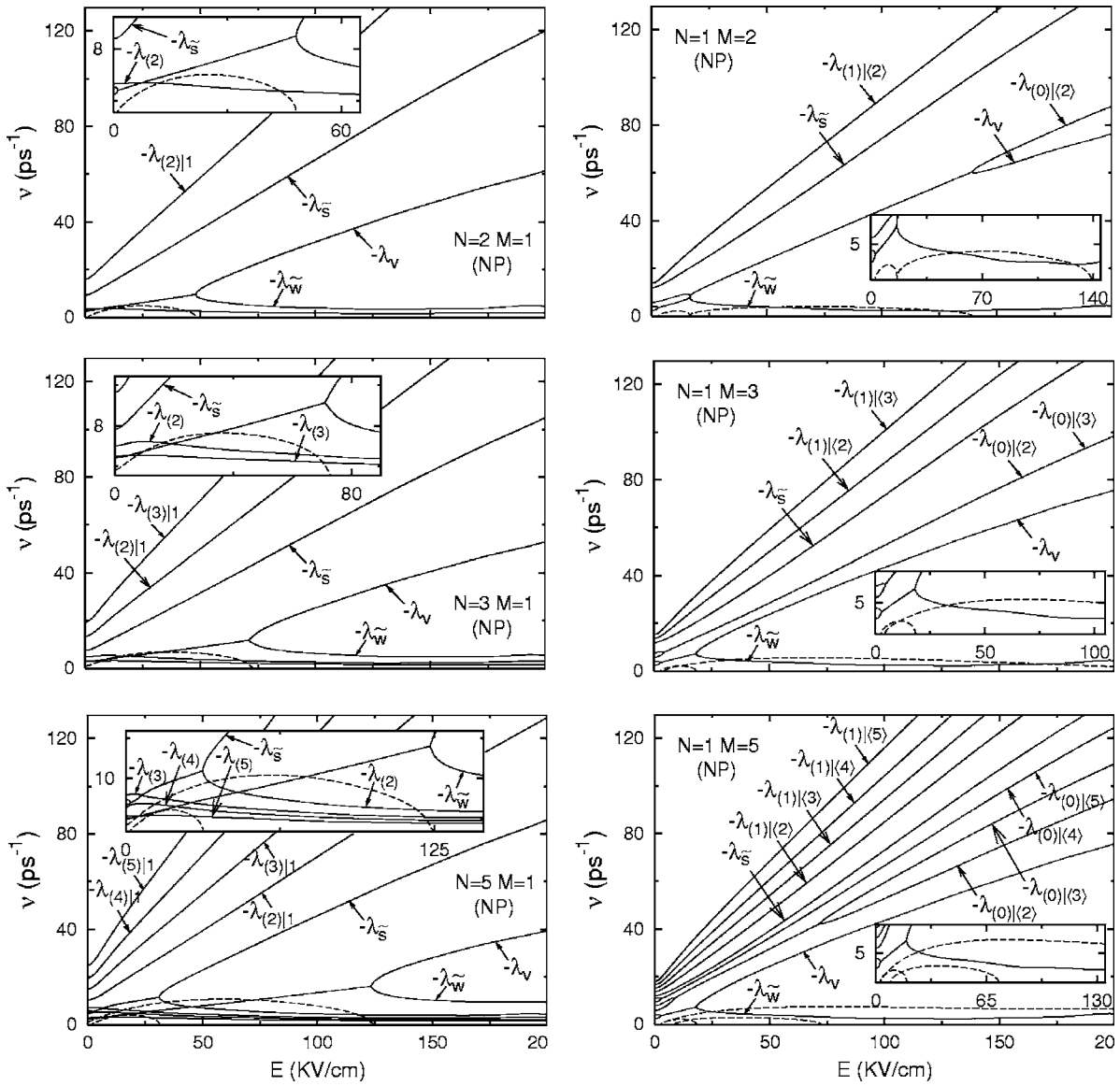

FIG. 3. Eigenvalues of the relaxation matrix vs electric field for electrons in Si in the nonparabolic (NP) band model at $T_0=300$ K. The continuous and the dashed lines (better evidenced in the insets) refer to the real and imaginary parts of the eigenvalues evaluated in the linear approximation for (on the left) a set of scalar and vectorial moments with $\{N=2,M=1\}$, $\{N=3,M=1\}$, and $\{N=5,M=1\}$ and for (on the right) a set of tensorial moments with $\{N=1,M=2\}$, $\{N=1,M=3\}$, and $\{N=1,M=5\}$, respectively.

scalar and vectorial moments used. As a matter of fact, for increasing values of N, we found that the generalized vectorial rates are squeezed towards lower values with the consequent extension of the coupling regions. In particular, for $N=5$ the spectrum of $\Gamma_{\alpha\beta}$ shows (see inserts of figures) another pair of complex conjugate eigenvalues ($-\lambda_{\tilde{s}}$ and $-\lambda_{(2)}$) with a coupling region smaller than that associated with velocity and energy relaxation. For the sake of comparison, the right part of Fig. 3 reports the eigenvalue spectrum of $\Gamma_{\alpha\beta}$ by taking $N=1$ (i.e., by fixing the isotropic part of moments) and varying the tensorial order $M=2,3,5$ (i.e., by considering moments with increasing deviatoric part). We can observe that all moments $\tilde{F}_{(0)|\langle s\rangle}$ show coupling regions with an extension that depends on the increasing tensorial order s. Therefore, in the low-field region, velocity and energy generalized relaxation rates are coupled by the electric field and analogously also the remaining generalized rates $\{\lambda_{(0)|\langle s\rangle}\}$ are found to be strongly coupled by exhibiting complex values that, in some cases, extend to the whole range of considered electric fields. These numerical results confirm the interpretation given above of the saturation regions shown in Fig. 1, that strong dissipative phenomena affect all moments $\tilde{F}_{(0)|\langle s\rangle}$ which have increasing values of the deviatoric part s. We have verified that, by considering a simultaneous increment of values N and M, the essential characteristics of the spectrum shown in Fig. 3 remain unchanged. Thus, for increasing values of the isotropic part N the spectrum of $\Gamma_{\alpha\beta}$ shows that all eigenvalues $\lambda_{(p)|\langle s\rangle}$ are squeezed towards lower values (as shown on the left of Fig. 3 for increasing N) with the consequent extension of all the coupling regions for the rates $\lambda_{(0)|\langle s\rangle}$ and the presence of other small regions (at low fields) with complex eigenvalues for some rates $\lambda_{(1)|\langle s\rangle}$.

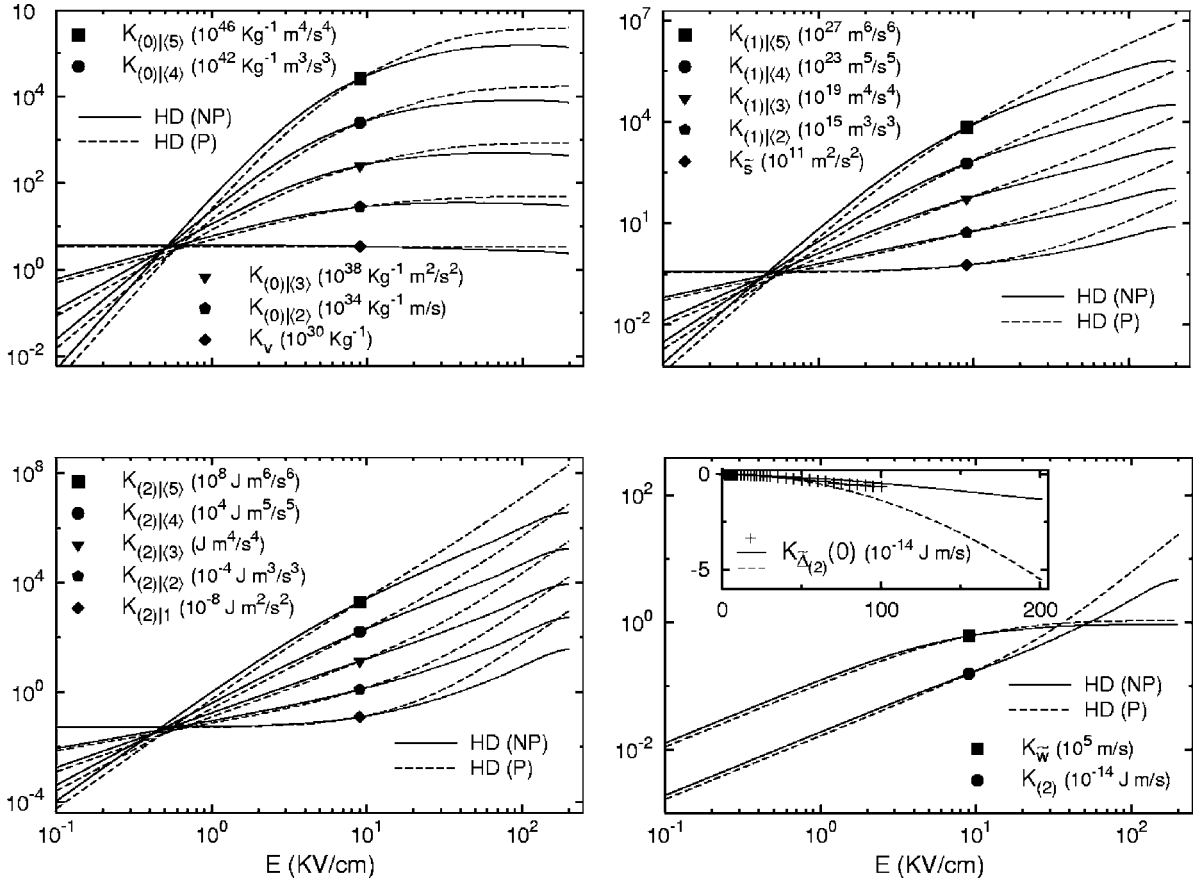

FIG. 4. Initial values ($t=0$) for the tensorial response functions $K_{(p)|\langle s\rangle}=\{K_{(0)|\langle s\rangle},K_{(1)|\langle s\rangle},K_{(2)|\langle s\rangle}\}$ (with $s=1,\ldots,5$) and for the scalar response functions $K_{(p)}=\{K_{\tilde{W}},K_{(2)},K_{\tilde{\Delta}_{(2)}}\}$ vs electric field for electrons in Si at $T_0=300$ K. Symbols refer to present parabolic (dashed lines) and nonparabolic (solid lines) HD calculations with $N=2$ and $M=5$. In particular for $K_{\tilde{\Delta}_{(2)}}(0)$ we report also the calculation (crosses) obtained by using in Eq. (44) the MC nonparabolic simulations (Ref. 56) for the moments $\{v,\tilde{W},\tilde{S}\}$.

It should be noted, that the dissipative processes associated with the streaming character of the transport have been evidenced in previous works[33,34,36,37,39,41,43] using only the usual HD equations for v and $\tilde{W}$ together with the relaxation time approximation. Although these results are similar to those obtained in the present work, yet there are same differences in the extension of the region where velocity and energy relaxations show to be strongly coupled. These differences are mainly attributed to the number of moments used to calculate the spectrum of $\Gamma_{\alpha\beta}$. Indeed, the eigenvalue spectrum is rather sensitive to the number of moments considered with the direct consequence of obtaining a much more pronounced extension of the coupling regions and of the number of coupled complex eigenvalues by increasing the number of moments. We conclude that under conditions very far from thermal equilibrium the variables $\{v,\tilde{W}\}$ alone no longer constitute a satisfactory set of relevant variables. Indeed, the analysis of the eigenvalue spectrum suggests that, for large values of the electric field, a detailed investigation of dissipative processes involve moments higher than the second one. Accordingly, the inclusion of a large number of moments is mandatory for an accurate description of the dissipation processes in the whole range of electric field strength.

C. Response functions and differential response

Figure 4 reports the initial values ($t=0$) of the response functions for the tensorial moments $\tilde{F}_{(p)|\langle s\rangle}$ (with $p=0,1,2$ and $s=1,\ldots,5$) and for the scalar moments $\{\tilde{W},\tilde{F}_{(2)},\tilde{\Delta}_{(2)}\}$ as a function of the electric field for parabolic and nonparabolic band models at $T_0=300$ K. As a general trend, hot-carrier effects (arising above about 1 kV/cm) are responsible for a systematic change in the bending of all the initial values $\{K_\alpha(0)\}$, which exhibit asymptotic behaviors steeper for higher moments. The net effect of band nonparabolicity is to systematically reduce the value of all the moments at high fields (see Fig. 1) and, according with analytic calculations of Eq. (42), also of the corresponding initial values of the response functions. Only the response functions $K_{(0)|\langle s\rangle}(0)$, at increasing electric fields, exhibit a saturation behavior that corresponds with the region of saturation for the moments $\tilde{F}_{(0)|\langle s-1\rangle}$. In particular, $K_v(0)=1/m^*$ remains almost constant in the whole range of values of E. Indeed, because of band nonparabolicity, all curves $K_{(0)|\langle s\rangle}(0)$ exhibit small changes at high fields due to increasing values of the carrier mass m^*, so that $K_{(0)|\langle s\rangle}(0)\propto 1/m^*\tilde{F}_{(0)|\langle s-1\rangle}$ slightly decrease. For the scalar moments [Eq. (42) with $s=0$] $K_{\tilde{W}}(0)$ saturates at high fields

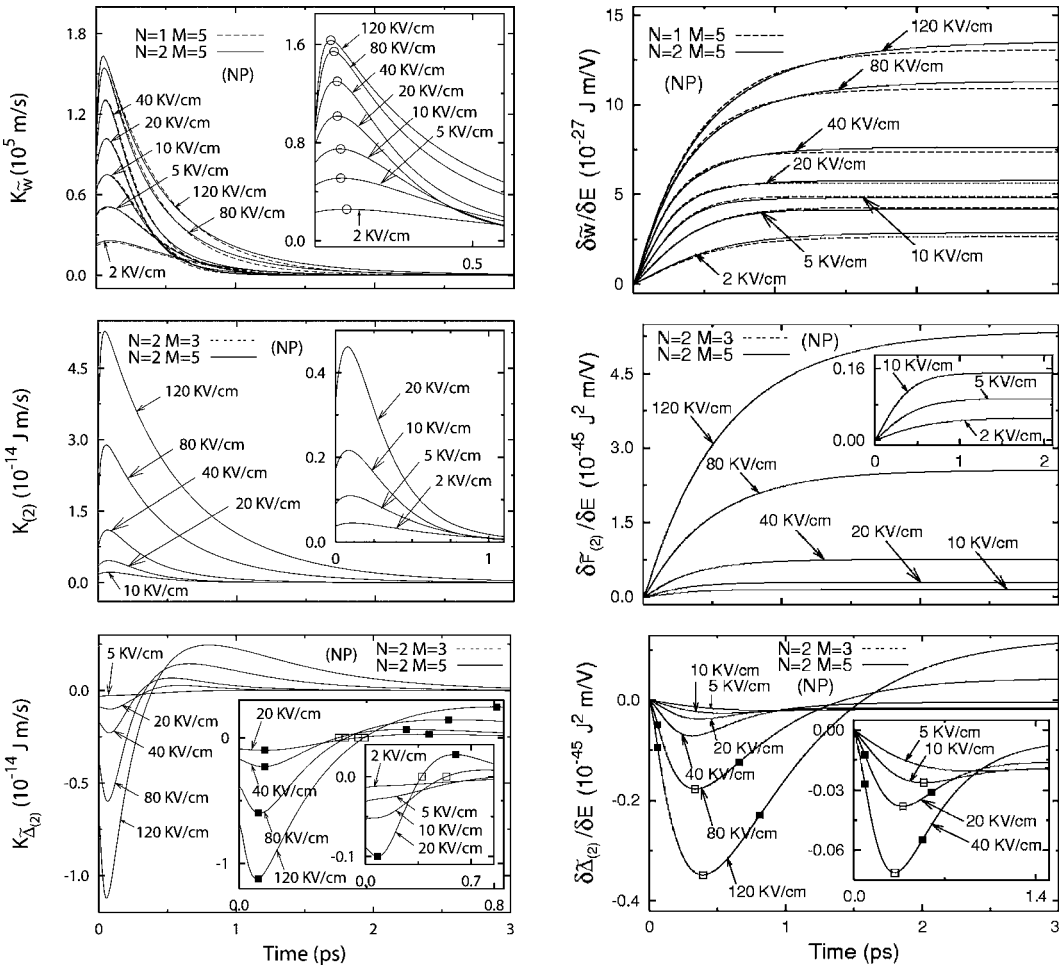

FIG. 5. Time dependencies of response function $\{K_{\tilde{w}}, K_{(2)}, K_{\tilde{\Delta}_{(2)}}\}$ and of corresponding differential response $\{\delta\tilde{w}/\delta E, \delta\tilde{F}_{(2)}/\delta E, \delta\tilde{\Delta}_{(2)}/\delta E\}$ to a steplike switch-on of the electric field obtained for n-Si in the case of a nonparabolic (NP) band model at $T_0=300$ K and increasing electric fields. The dashed and continuous lines refer to different number of moments used.

similar to the drift velocity v, while the moments $K_2(0)$ increase with the field proportionally to the energy flux $\tilde{S}$. In the insert of Fig. 4 we report also the response function $K_{\tilde{\Delta}_{(2)}}(0)$ obtained from Eq. (44) (with $l \propto 2$) by using HD and MC (Ref. 56) calculations for $\{v, \tilde{W}, \tilde{S}\}$. In this case, it should be noted that $K_{\tilde{\Delta}_{(2)}}(0)$ takes always negative values and it decreases monotonically with increasing fields both in the parabolic and nonparabolic band models.

Figure 5 reports the time dependence of the scalar-response functions $\{K_{\tilde{W}}, K_{(2)}, K_{\tilde{\Delta}_{(2)}}\}$ and of the corresponding differential response $\{\delta\tilde{W}/\delta E, \delta\tilde{F}_{(2)}/\delta E, \delta\tilde{\Delta}_{(2)}/\delta E\}$ to the steplike switching-on of the electric field for the nonparabolic band model and at increasing electric fields. The response function $K_{\tilde{W}}$ clearly evidences hot carriers effects through a nonmonotonic behavior with a maximum[45] (circles in the insert) which separates the initial ballistic regime from the subsequent diffusive regime where dissipation phenomena associated with the scattering take place. By contrast, the corresponding differential response $\delta\tilde{W}/\delta E$ increases systematically with field until reaching the steady-state value. In general, the response function of scalar moments exhibits a decay slower than that of the remaining tensorial moments, a behavior associated with the energy dependence of the scattering mechanisms considered here.[33,34,36] Thus, all the scalar response functions and the corresponding differential responses exhibit a time evolution analogous to that of the functions $K_{\tilde{W}}$ and $\delta\tilde{W}/\delta E$. As a matter of fact, being $\tilde{\Delta}_{(p)} \ll \tilde{F}_{(p)}|_E$ (see, for example, $\tilde{F}_{(2)}$ and $\tilde{\Delta}_{(2)}$ in Figs. 1 and 2), the evolution of the functions $K_{(p)}$ and $\delta\tilde{F}_{(p)}$ is mainly related to the equilibrium part $\tilde{F}_{(p)}|_E \propto \tilde{W}^p$ of the scalar moments. Accordingly, all the $K_{(p)}$ functions show a nonmonotonic behavior (with a steep initial increase, the attainment of a maximum, and a successive slow decay) that evolves approximately with the same time scales of the curves associated with the response function $K_{\tilde{W}}$. The corresponding differential responses $\delta\tilde{F}_{(p)}/\delta E$ exhibit a behavior similar to that of the function $\delta\tilde{W}/\delta E$, with a monotonous time variation for all the values of the electric field. Figure 5 also reports the functions $K_{\tilde{\Delta}_{(2)}}$ and $\delta\tilde{\Delta}_{(2)}/\delta E$, which are associated with the nonequilibrium moment $\tilde{\Delta}_{(2)}$. In particular, $K_{\tilde{\Delta}_{(2)}}(t)$ is initially negative and then decreases, at very short

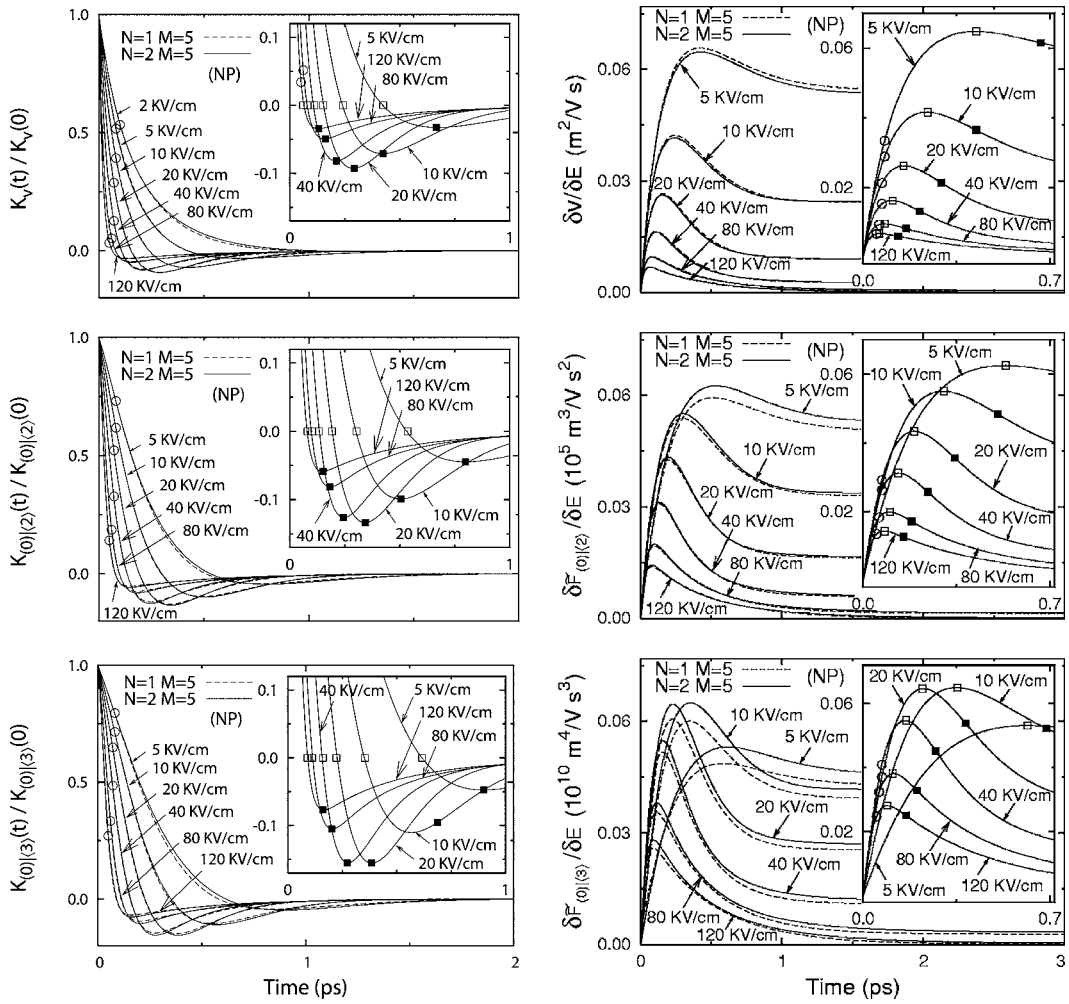

FIG. 6. Time dependencies of normalized response functions $\{K_v, K_{(0)|\langle 2\rangle}, K_{(0)|\langle 3\rangle}\}$ and of corresponding differential response $\{\delta v/\delta E, \delta\tilde{F}_{(0)|\langle 2\rangle}/\delta E, \delta\tilde{F}_{(0)|\langle 3\rangle}/\delta E\}$ to a steplike switch-on of the electric field obtained for *n*-Si in the case of a nonparabolic (NP) band model at $T_0=300$ K and increasing electric fields. The dashed and continuous lines refer to different number of moments used.

times, to a minimum before increasing towards its null value and, in case of high electric fields, it becomes positive and relaxes slowly towards zero. Analogously, for every value of the electric field, the corresponding differential response $\delta\tilde{\Delta}_{(2)}/\delta E$ quickly decreases, reaches a negative minimum and slowly relaxes to the value of the steady state. The shape of the functions $\{K_{\tilde{\Delta}_{(2)}}, \delta\tilde{\Delta}_{(2)}\}$ is consistent with the relations (29), (31) and (22), (23). Indeed, for every value of the electric field $K_{\tilde{\Delta}_{(2)}}(0)$ is always negative (see insert in Fig. 4) while for $E>20$ KV/cm the dc differential mobility (see Fig. 2) takes always non-negative values. From Eqs. (29) and (31) we obtain that, in these conditions, the integral of $K_{\tilde{\Delta}_{(2)}}(t)$ over all times is generally non-negative, so that positive values of the integrand must dominate. Therefore, being $K_{\tilde{\Delta}_{(2)}}$ initially negative, at later times it must transit from a zero to positive values with increasing time. If in the transition point the derivative $dK_{\tilde{\Delta}_{(2)}}/dt$ is strictly positive then, from Eqs. (22) and (23), we obtain that to a zero of the response function it corresponds a minimum of the differential response (open squares in the inserts of Fig. 5), and analogously, to flex points of $\delta\tilde{\Delta}_{(2)}$ (full squares in the insets of Fig. 5) one can associate the extreme positions for the corresponding response function $K_{\tilde{\Delta}_{(2)}}$.

Figure 6 reports the response functions $K_{(p)|\langle s\rangle}$ (for $p=0$ and $s=1,2,3$) and the corresponding differential response $\delta\tilde{F}_{(p)|\langle s\rangle}/\delta E$ to a steplike switch-on of the electric field for the nonparabolic band model at increasing electric fields. Each curve $K_{(p)|\langle s\rangle}$ is normalized to its initial value to allow for a comparison of the different decay-time scales. The results show that, at increasing values of the deviatoric part *s*, all functions $\{K_{(0)|\langle s\rangle}, \delta\tilde{F}_{(0)|\langle s\rangle}/\delta E\}$ exhibit a time evolution very similar to that of the functions $\{K_v, \delta v/\delta E\}$ for the velocity *v*. Accordingly, at the lowest fields all the response functions $K_{(0)|\langle s\rangle}$ exhibit an exponential decay, with a relaxation time characteristic of the corresponding moment $\tilde{F}_{(0)|\langle s\rangle}$. The presence of higher electric fields induces nonexponential decays. Accordingly, the shape of all functions $K_{(0)|\langle s\rangle}$ becomes more complicate by exhibiting a negative part that implies an overshoot of the corresponding differential response. Thus, the responses $\delta\tilde{F}_{(0)|\langle s\rangle}/\delta E$ quickly increase with time when

$K_{(0)|\langle s\rangle}(t)>0$, reach a maximum at time $\bar{t}$ corresponding to $K_{(0)|\langle s\rangle}(\bar{t})=0$, and then decay asymptotically to zero when $K_{(0)|\langle s\rangle}(t)<0$. We note that, also in this case, from Eqs. (29) and (31) one can infer the relevant features of the response functions. In fact, by considering the regions of saturation (see Fig. 1) for the moments $\tilde{F}_{(0)|\langle s\rangle}$, from Eq. (29) we obtain that $X_{(0)|\langle s\rangle}(0)$ decreases to zero and the integral in Eq. (31) vanishes for high fields. Thus, if the initial part of the response functions is positive (see Fig. 4), then at long times the contribution of the integrand in Eq. (31) should be negative to compensate. In this transition, the response functions fall through a zero and the corresponding derivative becomes negative. In particular, if at the transition point it is $dK_{(0)|\langle s\rangle}/dt<0$, then, from Eqs. (22) and (23), to a zero value of $K_{(0)|\langle s\rangle}$ it corresponds a positive maximum of $\delta\tilde{F}_{(0)|\langle s\rangle}$ (open squares in the insets of Fig. 6), and analogously, to one flex point of the perturbation $\delta\tilde{F}_{(0)|\langle s\rangle}$ (full squares in the insets of Fig. 6) can be associated an extreme position of the corresponding response function. We remark that, for continuity reasons, the previous behavior of the functions $K_{(0)|\langle s\rangle}(E,t)$ must be valid also in some range of intermediate dc electric fields. Of course, being in this case, $X_{(0)|\langle s\rangle}(E,0)>0$, the positive values of the integrand in Eq. (31) must predominate. According with the previous interpretation, this phenomenon is associated with the combined action of the electric field and dissipative processes. At the very beginning, the field accelerates the electron gas, and all the particles will move toward the region of energy where phonon emission becomes possible. In this time interval ($t\approx 0-0.1$ ps) we are in the presence of a ballistic regime, and the perturbations of the mean velocity and remaining moments increase linearly with time. The fastest electrons will then emit optical phonons, becoming in this way very slow, and in turn all perturbations $\delta\tilde{F}_{(0)|\langle s\rangle}$ will tend to level off. Later on, as an effect of the scattering, fast electrons (those which have not yet undergone scattering) separate from slow electrons (which did undergo scattering) thus causing a decrease of all perturbations $\delta\tilde{F}_{(0)|\langle s\rangle}$ after they achieved their maximum value. Finally, due to the randomness of the scattering, both δv and remaining functions $\delta\tilde{F}_{(0)|\langle s\rangle}$ (for $s>1$) reach their steady-state value. As previously noted, the streaming character of the transport is also evidenced by the nonmonotonic behavior of $K_{\tilde{W}}$, which exhibits a maximum separating the ballistic regime from the dissipation regime of hot carriers. In fact, $K_{\tilde{W}}$ is always positive with a maximum which is reached at times t' shorter than that of the zero value of $K_{(0)|\langle s\rangle}$ (see circles in the insets of Fig. 6). At increasing fields, because of the increased efficiency of the scattering mechanisms, the corresponding value $K_{(0)|\langle s\rangle}(t')$ tends to approach the value $K_{(0)|\langle s\rangle}(\bar{t})=0$ and analogously the corresponding value of $\delta\tilde{F}_{(0)|\langle s\rangle}(t')/\delta E$ tends to approach its maximum value. Therefore, if initially the tensorial moments $\tilde{F}_{(0)|\langle s\rangle}$ receive an extra contribution gained by the field then, due to scattering, at a later time the corresponding perturbations $\delta\tilde{F}_{(0)|\langle s\rangle}/\delta E$ reach their maximum, decreases, and the extra contributions for the moment $\tilde{F}_{(0)|\langle s\rangle}$ disappear.

For the remaining tensorial moments $\tilde{F}_{(p)|\langle s\rangle}$ (with $p\geq 1$), even in the absence of the overshoot phenomena, we have verified that a relaxation decay based on a single time scale does not work, rather each function exhibits different time scales. Consistently with the interpretation reported in Secs. V A and V B, the evolutions exhibited by the response functions and by the differential responses are the consequence of the competition between the actions of electric field and of scattering mechanisms. A general property common to all the results is that, for larger values of the deviatoric part s, the functions $K_{(p)|\langle s\rangle}$ exhibit a more pronounced negative region and analogously a more pronounced peak in the corresponding differential responses $\delta\tilde{F}_{(p)|\langle s\rangle}/\delta E$. Again, these behaviors are mainly attributed to the prevailing importance of the scattering mechanisms at increasing values of the deviatoric part of the moments. By contrast, for increasing values of the moment isotropic part (i.e., larger values of the index p), the negative regions of the response functions are reduced. In many cases, for high electric fields the functions $K_{(p)|\langle s\rangle}$ are always positive and any overshoot phenomenon in the corresponding perturbations $\delta\tilde{F}_{(p)|\langle s\rangle}/\delta E$ is washed out. Also in these cases, near to the maximum of $K_{\tilde{W}}$ the shape of the curves exhibits an abrupt change in the temporal evolution of both the response function and the differential response. This behavior is mainly attributed to the prevailing importance of the action of the electric field since, in this case, energy dissipation is not sufficient to counteract the energy supplied by field.

We conclude that, the shape of all the curves evidences the streaming character of the transport exhibiting different decay-time scales. In particular, the response function $K_{\tilde{W}}$ in Fig. 5 evidences the presence of hot carriers effects through a nonmonotonic behavior with a maximum which separates the different time scales. Finally, for increasing fields we note that, while the introduction of a greater number of moments yields small differences in the HD numerical results, the introduction of nonparabolicity leads to a remarkable variation in the values of all the functions, with more pronounced negative minima in the response functions.

D. Differential mobility

The previous section has shown that the structure of the response functions provides much information on the physics of the system. In general, however, the response functions are not directly measurable quantities. Therefore, in this section we present the implications of previous results for the generalized differential mobilities, which for the case of velocity mobility is directly accessible by measurements of the differential mobility spectrum,[28] while the remaining quantities can be calculated by different numerical approaches.[30,39,40,45] Accordingly, Fig. 7 reports the low frequency differential mobility $\{\mu_v', \mu_{\tilde{W}}', \mu_{\tilde{S}}'\}$, for the moments $\{v, \tilde{W}, \tilde{S}\}$, as a function of the electric field at $T_0=300$ K. We note, that in the nonparabolic case the HD results are in good

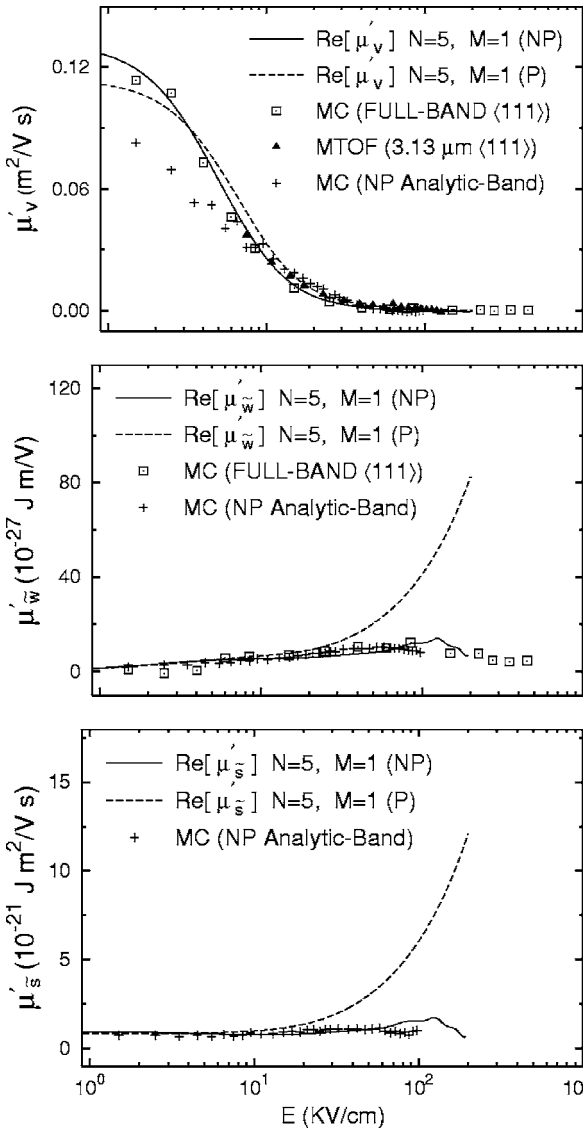

FIG. 7. Real parts of the ac differential mobility for velocity, energy, and energy flux vs electric field E at low frequency $\approx 10^8$ Hz obtained with the present HD approach. Lines refer to present parabolic and nonparabolic model calculations obtained, with $N=5$ and $M=1$. Symbols refer to full-band MC simulations (Ref. 57), to experimental data (Refs. 32 and 58) measured with the microwave time-of-flight (MTOF) method and to nonparabolic-band MC simulations (Ref. 56) performed along the ⟨111⟩ crystallographic direction for n-Si.

agreement with both MC calculations and experimental data for the whole range of electric fields.

As further test of the HD model, we have also calculated the differential velocity-mobility at high frequency for $T_0=293$ K. Accordingly, in Fig. 8 we compare the HD results with the experimental data[28] for the real part of the velocity-mobility μ_v' obtained at 123.3 GHz as a function of the electric field. More precisely, the HD simulations have been performed for the parabolic (P) and nonparabolic (NP) band models with $N=5$ and $M=1$. We remark that the nonparabolic HD results agree very well with experimental data.

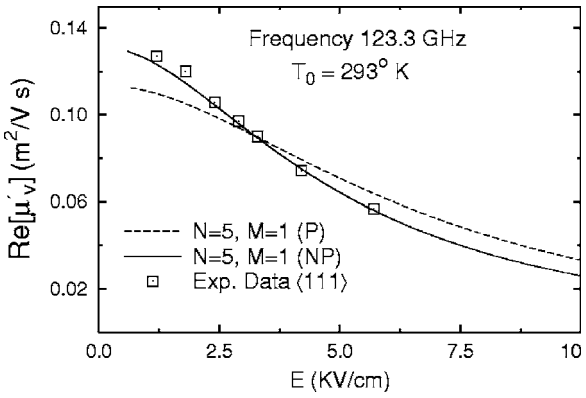

FIG. 8. Real parts of the ac differential mobility for velocity ($\mathrm{Re}[\mu_v'(f)]$) at $T=293$ K evaluated at high frequency (123.3 GHz), as function of low electric fields E, with the present HD approach. Lines refer to present parabolic and nonparabolic model calculations obtained for $N=5$, $M=1$. Symbols refer to the experimental data (Ref. 28) measured with the microwave time-of-flight (MTOF) technique along the ⟨111⟩ crystallographic direction for n-Si.

In general we have verified that, if the curves $K_{(p)|\langle s\rangle}$ for different values of indices p and s show common features, then also the ac differential mobility $\mu'_{(p)|\langle s\rangle}$ show in correspondence similar common features. Accordingly, if the negative parts of the response functions $K_{(p)|\langle s\rangle}$ are predominant in the time domain (see Fig. 6), then at increasing frequencies all curves $\mathrm{Re}[\mu'_{(p)|\langle s\rangle}]$ exhibit a peak before falling off to zero. Analogously, all the imaginary parts $\mathrm{Im}[\mu'_{(p)|\langle s\rangle}]$ increase through a positive maximum before decreasing toward a negative minimum. Even in the absence of negative parts in $K_{(p)|\langle s\rangle}$, the shape of the curves $\mu'_{(p)|\langle s\rangle}$ are found to evidence the existence of two different decay-time scales in the response functions.

VI. CONCLUSIONS

By introducing generalized kinetic fields we have developed an extended HD approach based on the maximum entropy principle, which includes an arbitrary number of moments of the distribution function. Then, for the perturbation of these moments a set of coupled balance equations is constructed and analytical expressions for all the small signal coefficients are obtained in the time and frequency domains. In particular, the generalized expressions for the response matrix $\Gamma_{\alpha\beta}$, the perturbing forces $-e\delta E\xi(t)\Gamma_\alpha^{(E)}$, the response functions $K_\alpha(t)$, and the differential mobilities $\mu'_\alpha(\omega)=X_\alpha(\omega)+iY_\alpha(\omega)$ are directly calculated for any moment of interest. By generalizing previous results, the theory provides also some relations in integral form and in asymptotic form that are used to describe the small signal analysis. From the knowledge of the quantities $\{K_\alpha(0), X_\alpha(0)\}$ and of the derivatives $[dK_\alpha/dt]_{0+}$, $[d^2K_\alpha/dt^2]_{0+}$, $[dY_\alpha/d\omega]_0$, $[d^2X_\alpha/d\omega^2]_0$ the anatomy of all response functions and differentials mobilities is inferred in the time and frequency domains. The power of the present approach stems from the construction of an algebraic (in place of an integral) formulation of the theory.

Thus, from the explicit knowledge of $\{\Gamma_{\alpha\beta},\Gamma_{\alpha}^{(E)}\}$ the small signal coefficients are consistently obtained in algebraic form.

The theory is formulated at a kinetic level, without the need to introduce external parameters, and it has been carried out within a total energy scheme, thus using an energy dispersion of general form (full-band approach). The physical plausibility of the theory has been confirmed by analysing the high field transport in *n*-Si. To this purpose, as generalized kinetic fields we have taken the independent quantities $\Psi_{\alpha}=\{\varepsilon^{p}u_{\langle i_1}\cdots u_{i_s\rangle}\}$ and as unique independent mean quantities the traceless moments $F_{\alpha}=\{F_{(p)|\langle i_1\cdots i_s\rangle}\}$, where the indices p and s are associated with the isotropic and deviatoric parts of the tensors, respectively. The analysis of dc and ac numerical results shows that the behavior of all moments is determined essentially by the competition between the action of the electric field and that of the dissipative scattering processes. In particular, the action of the electric field prevails on the moments which have an increasing isotropic part while the action of dissipative processes are more evident in the moments with a large deviatoric part. By studying the eigenvalues and eigenvectors of the response matrix we have analyzed the coupling among the different macrovariables (moments) and we have found that this coupling leads to a nonexponential decay of the corresponding response functions. In particular, by considering the moments $F_{(0)|\langle s\rangle}$, with null isotropic part and increasing deviatoric part, the combined action of the electric field and dissipative processes has been quantitatively investigated. We have thus demonstrated that, at high fields: (i) the vanishing dc differential mobility of different moments, (ii) the presence of complex eigenvalues, (iii) the negative values taken by the response functions, (iv) the positive overshoot of differentials responses, and (v) the maximum of the real and imaginary parts of the ac differentials mobility, are all related to the efficiency of dissipative scattering processes. Analogously, by considering the moments $F_{(p)|\langle s\rangle}$ with increasing isotropic part ($p\geq 1$) we have established that a simple relaxation approach based on a single time scale loses of validity, because both the response functions and the corresponding differential responses evolve with different time scales. In particular, the energy response function $K_{\tilde{W}}$ evidences the streaming character of hot carriers through a nonmonotonic behavior with a maximum which separates different time scales. The limits of the concept of a single relaxation time are also evident in the shape of the corresponding ac differential mobilities which show a nonregular behavior at increasing frequencies before reaching the cutoff. The theory has been validated by comparing the present results with those obtained from MC simulations and with available experiments for the standard quantities of direct physical interpretation $\{v,\tilde{W},\tilde{S}\}$. Therefore, we believe that the present approach represents a useful standard to obtain a generalized modeling of the relevant static macrovariables of interest and of the small-signal (dynamics) coefficients in terms of rigorous analytical formulas associated with microscopic peculiarities of the single carrier transport. In addition to offering an approach complementary to existing kinetic method based on Monte Carlo simulations and/or iterative solutions of the Boltzmann equation, the theory has the advantages of providing a systematic framework to investigate transport phenomena under far from equilibrium conditions and of operating within a contained computational environment.

ACKNOWLEDGMENTS

M. V. Fischetti, T. Gonzales, and M. J. Martin are thanked for providing the MC data. One of us (M.T.) acknowledges T. Steger for helpful discussions. Partial support from GNFM-INDAM and MADESS II project of the Italian National Research Council (CNR) is gratefully acknowledged.

APPENDIX

The components of the vector $\mathbf{\Gamma}^{(E)}$

$$\Gamma_{\alpha}^{(E)}=\{\Gamma_{(q)}^{(E)},\Gamma_{(p)|1}^{(E)},\Gamma_{(p)|\langle 2\rangle}^{(E)},\ldots,\Gamma_{(p)|\langle s\rangle}^{(E)},\ldots,\Gamma_{(p)|\langle M\rangle}^{(E)}\}^{T},$$

are expressed in terms of relations

$$\Gamma_{(q)}^{(E)}=q\tilde{F}_{(q-1)|1}, \tag{A1}$$

$$\Gamma_{(p)|1}^{(E)}=\frac{(2p+3)}{3}\frac{1}{m^{*}}\tilde{F}_{(p)}+p\tilde{F}_{(p-1)|\langle 2\rangle},\ldots, \tag{A2}$$

$$\Gamma_{(p)|\langle s\rangle}^{(E)}=\frac{s^2}{2s-1}\left\{\frac{2(s+p)+1}{2s+1}\frac{1}{m^{*}}\tilde{F}_{(p)|\langle s-1\rangle}\right\}+p\tilde{F}_{(p-1)|\langle s+1\rangle},\ldots, \tag{A3}$$

$$\Gamma_{(p)|\langle M\rangle}^{(E)}=\frac{M^2}{2M-1}\left\{\frac{2(M+p)+1}{2M+1}\frac{1}{m^{*}}\tilde{F}_{(p)|\langle M-1\rangle}\right\}, \tag{A4}$$

with $q=1,\ldots,N$ and $p=0,\ldots,N$.

All the elements $\mathbf{\Gamma}_{w}^{(s)}$ of the first column of the matrix (47) are vectors

$$\mathbf{\Gamma}_{w}^{(0)}=\{\Gamma_{(1)},\Gamma_{(2)},\ldots,\Gamma_{(N)}\}^{T},$$

$$\mathbf{\Gamma}_{w}^{(1)}=\{\Gamma_{(0)|1},\Gamma_{(1)|1},\ldots,\Gamma_{(N)|1}\}^{T},$$

$$\mathbf{\Gamma}_{w}^{(s)}=\{\Gamma_{(0)|\langle s\rangle},\Gamma_{(1)|\langle s\rangle},\ldots,\Gamma_{(N)|\langle s\rangle}\}^{T},\quad \text{with } s=2,\ldots,M$$

of components

$$\Gamma_{(q)}=qeE\frac{\mu'_{(q-1)|1}+\mu_{(q-1)|1}}{\mu'_{w}}+\sum_{l=2}^{N}\alpha_{ql}^{(0)}\frac{\mu'_{(l)}}{\mu'_{w}},\quad \text{for } q=1,\ldots,N, \tag{A5}$$

$$\Gamma_{(0)|1}=\sum_{r=0}^{N}\alpha_{0r}^{(1)}\frac{\mu'_{(r)|1}-\mu_{(r)|1}}{\mu'_{w}}, \tag{A6}$$

$$\Gamma_{(1)|1}=\sum_{r=0}^{N}\alpha_{1r}^{(1)}\frac{\mu'_{(r)|1}-\mu_{(r)|1}}{\mu'_{w}}+eE\frac{\mu'_{(0)|\langle 2\rangle}}{\mu'_{w}}, \tag{A7}$$

$$\Gamma_{(n)|1} = \sum_{r=0}^{N} \alpha_{nr}^{(1)} \frac{\mu'_{(r)|1} - \mu_{(r)|1}}{\mu'_w} + eE\left\{ n \frac{\mu'_{(n-1)|\langle 2\rangle}}{\mu'_w} + \frac{2n+3}{3} \frac{1}{m^*} \frac{\mu'_{(n)}}{\mu'_w} \right\} \quad \text{for } n = 2, \ldots, N \tag{A8}$$

$$\Gamma_{(p)|\langle s\rangle} = eE\left\{ p \frac{\mu'_{(p-1)|\langle s+1\rangle}}{\mu'_w} + \frac{s^2}{2s-1}\left[\frac{2(p+s)+1}{2s+1}\right]\frac{1}{m^*}\frac{\mu'_{(p)|\langle s-1\rangle}}{\mu'_w} \right\} + \sum_{r=0}^{N} \alpha_{pr}^{(s)} \frac{\mu'_{(r)|\langle s\rangle} - \mu_{(r)|\langle s\rangle}}{\mu'_w}$$

$$\text{for } p = 0, \ldots, N,\ s = 2, \ldots, M, \text{ and } \mu'_{(p)|\langle M+1\rangle} = 0, \tag{A9}$$

where

$$\mu_{(p)|1} = \frac{\tilde{F}_{(p)|1}}{E}, \ldots, \mu_{(p)|\langle s\rangle} = \frac{\tilde{F}_{(p)|\langle s\rangle}}{E}, \ldots, \mu_{(p)|\langle M\rangle} = \frac{\tilde{F}_{(p)|\langle M\rangle}}{E}, \quad \text{for } p = 0, \ldots, N \tag{A10}$$

are the moments generalized chord mobility and

$$\mu'_w = \frac{d\tilde{W}}{dE}, \quad \mu'_{(l)} = \frac{d\tilde{F}_{(l)}}{dE},$$

$$\mu'_{(p)|1} = \frac{d\tilde{F}_{(p)|1}}{dE}, \ldots, \mu'_{(p)|\langle s\rangle} = \frac{d\tilde{F}_{(p)|\langle s\rangle}}{dE},$$

$$\text{for } l = 2, \ldots, N,\ p = 0, \ldots, N, \text{ and } s = 2, \ldots, M \tag{A11}$$

are the moments generalized differential mobility.

The submatrices $\{\mathbf{A}^{(s)}, \mathbf{B}^{(r)}, \mathbf{C}^{(n)}\}$ contained in the response matrix (47) are expressed in terms of coefficients $\alpha_{ql}^{(s)}$ and of electric field E. In particular we have for the $N \times (N-1)$ matrix $\mathbf{A}^{(0)}$ and for the $(N+1)\times(N+1)$ matrix $\mathbf{A}^{(s)}$ (with $s = 1, \ldots, M$) the relations

$$\mathbf{A}^{(0)} = -\alpha_{qr}^{(0)} \quad \text{for } q = 1, \ldots, N,\ r = 2, \ldots, N \tag{A12}$$

$$\mathbf{A}^{(s)} = -\alpha_{nm}^{(s)} \quad \text{for } n, m = 0, \ldots, N. \tag{A13}$$

For the $N \times (N+1)$ matrix $\mathbf{B}^{(0)}$ and for the $(N+1)\times(N+1)$ matrix $\mathbf{B}^{(r)}$ (with $r = 1, \ldots, M-1$) the relations

$$\mathbf{B}^{(0)} = \begin{bmatrix} -eE & 0 & \cdots & 0 & 0 \\ 0 & -2eE & \cdots & 0 & 0 \\ \vdots & \vdots & \cdots & \vdots & \vdots \\ 0 & 0 & \cdots & -NeE & 0 \end{bmatrix},$$

$$\mathbf{B}^{(r)} = \begin{bmatrix} 0 & 0 & \cdots & 0 & 0 \\ -eE & 0 & \cdots & 0 & 0 \\ 0 & -2eE & \cdots & 0 & 0 \\ \vdots & \vdots & \cdots & \vdots & \vdots \\ 0 & 0 & \cdots & -NeE & 0 \end{bmatrix}. \tag{A14}$$

For the $(N+1)\times(N-1)$ matrix $\mathbf{C}^{(1)}$ and for the $(N+1)\times(N+1)$ matrix $\mathbf{C}^{(s)}$ (with $s = 2, \ldots, M$) the relations

$$\mathbf{C}^{(1)} = \begin{bmatrix} 0 & 0 & \cdots & 0 \\ 0 & 0 & \cdots & 0 \\ -\frac{7}{3}\frac{eE}{m^*} & 0 & \cdots & 0 \\ 0 & -\frac{9}{3}\frac{eE}{m^*} & \cdots & 0 \\ \vdots & \vdots & \cdots & \vdots \\ 0 & 0 & \cdots & -\frac{2N+3}{3}\frac{eE}{m^*} \end{bmatrix}, \tag{A15}$$

$$\mathbf{C}^{(s)} = \begin{bmatrix} -\frac{s^2}{2s-1}\frac{eE}{m^*} & 0 & \cdots & 0 \\ 0 & -\frac{s^2}{2s-1}\left[\frac{2(1+s)+1}{2s+1}\right]\frac{eE}{m^*} & \cdots & 0 \\ \vdots & \vdots & \cdots & \vdots \\ 0 & 0 & \cdots & -\frac{s^2}{2s-1}\left[\frac{2(N+s)+1}{2s+1}\right]\frac{eE}{m^*} \end{bmatrix}. \tag{A16}$$

[1] I. Müller and T. Ruggeri, *Rational Extended Thermodynamics*, Vol. 37 of Springer Tracts in Natural Philosophy (Springer-Verlag, New York, 1998).
[2] W. Weiss, Phys. Rev. E **52**, R5760 (1995).
[3] M. Trovato and P. Falsaperla, Phys. Rev. B **57**, 4456 (1998); **57**, 12617(E) (1998).
[4] M. Trovato and L. Reggiani, J. Appl. Phys. **85**, 4050 (1999).
[5] M. Trovato, P. Falsaperla, and L. Reggiani, J. Appl. Phys. **86**, 5906 (1999).
[6] H. Struchtrup, Physica A **275**, 229 (2000).
[7] S. F. Liotta and H. Struchtrup, Solid-State Electron. **44**, 95 (2000).
[8] M. Trovato and L. Reggiani, Phys. Rev. B **61**, 16667 (2000).
[9] M. Trovato and L. Reggiani, VLSI Des. **13**, 381 (2001).
[10] G. Mascali and M. Trovato, Physica A **310**, 121 (2002).
[11] M. Rudan, M. Vecchi, and D. Ventura, *Mathematical Problems in Semiconductor Physics*, Vol. 186 of Pitman Research Notes, Mathematics Series, edited by P. Marcati, P. Markowich, and R. Natalini (Longman, New York, 1995).
[12] E. T. Jaynes, Phys. Rev. **106**, 620 (1957).
[13] *Maximum Entropy and Bayesian Methods*, edited by J. Skilling (Cambridge, England, 1988).
[14] D. Jou, J. Casas-Vasquez, and G. Lebon, *Extended Irreversible Thermodynamics* (Springer-Verlag, Berlin, 1993).
[15] L. R. Mead and N. Papanicolaou, J. Math. Phys. **25**, 2404 (1984).
[16] A. E. Carlsson and P. A. Fedders, Phys. Rev. B **34**, 3567 (1986).
[17] D. A. Drabold and G. L. Jones, J. Phys. A **24**, 4705 (1991).
[18] D. A Drabold and O. F. Sankey, Phys. Rev. Lett. **70**, 3631 (1993).
[19] A. N. Gorban and I. V. Karlin, Phys. Rev. E **54**, R3109 (1996).
[20] I. V. Karlin, A. N. Gorban, S. Succi, and V. Boffi, Phys. Rev. Lett. **81**, 6 (1998).
[21] G. Drobny and V. Buzek, Phys. Rev. A **65**, 053410 (2002).
[22] S. Kiatgamolchai, M. Myronov, O. A. Mironov, V. G. Kantser, E. H. C. Parker, and T. E. Whall, Phys. Rev. E **66**, 036705 (2002).
[23] K. Bandyopadhyay, A. K. Bhattacharya, Parthapratim Biswas, and D. A. Drabold, Phys. Rev. E **71**, 057701 (2005).
[24] R. Landauer, Physica A **194**, 551 (1993).
[25] In Refs. 3 and 7 the authors showed a comparison between the MEP distribution function with those obtained by other methods. In Ref. 3 the MEP is used in a strong nonlinear dynamical context, for the hot carriers in submicrometric Si devices, in terms of first 13 moments. In Ref. 7, under spatially homogeneous conditions, the authors consider a Grad type approach, perfectly equivalent to the linearized MEP, in terms of increasing number of moments, for the Si bulk.
[26] V. Gruzhinskis, E. Starikov, P. Shiktorov, L. Reggiani, and L. Varani, J. Appl. Phys. **76**, 5260 (1994).
[27] E. Starikov, P. Shiktorov, V. Gruzhinskis, T. Gonzalez, M. J. Martin, D. Pardo, L. Reggiani, and L. Varani, Semicond. Sci. Technol. **11**, 865 (1996).
[28] J. Zimmermann, Y. Leroy, and E. Constant, J. Appl. Phys. **49**, 3378 (1978).
[29] P. Das and D. K. Ferry, Solid-State Electron. **19**, 851 (1976).
[30] P. J. Price, J. Appl. Phys. **53**, 8805 (1982).
[31] P. J. Price, J. Appl. Phys. **54**, 3616 (1983).
[32] L. Reggiani, *Hot-Electron Transport in Semiconductors*, Topics in Applied Physics Vol. 58 (Springer-Verlag, Berlin, 1985).
[33] P. Lugli, L. Reggiani, and J. J. Niez, Phys. Rev. B **40**, 12382 (1989).
[34] T. Kuhn, L. Reggiani, and L. Varani, Phys. Rev. B **42**, 11133 (1990).
[35] J. P. Nougier, *III-V Microelectronics*, edited by J. P. Nougier (North-Holland, Amsterdam, 1991), pp. 1–56.
[36] T. Kuhn, L. Reggiani, and L. Varani, Phys. Rev. B **45**, 1903 (1992).
[37] V. Gruzhinskis, E. Starikov, P. Shiktorov, L. Reggiani, M. Saranniti, and L. Varani, Semicond. Sci. Technol. **8**, 1283 (1993).
[38] V. Gruzhinskis, E. Starikov, and P. Shiktorov, Solid-State Electron. **36**, 1055 (1993).
[39] V. Gruzhinskis, E. Starikov, and P. Shiktorov, Solid-State Electron. **36**, 1067 (1993).
[40] J. C. Vaissiere, J. P. Nougier, L. Varani, P. Houlet, L. Hlou, E. Starikov, P. Shiktorov, and L. Reggiani, Phys. Rev. B **49**, 11144 (1994).
[41] L. Varani, J. C. Vaissiere, J. P. Nougier, P. Houlet, L. Reggiani, E. Starikov, P. Shiktorov, V. Gruzhinskis, and L. Hlou, J. Appl. Phys. **77**, 665 (1995).
[42] P. Golinelli, L. Varani, and L. Reggiani, Phys. Rev. Lett. **77**, 1115 (1996).
[43] L. Reggiani, E. Starikov, P. Shiktorov, V. Gruzhinskis, and L. Varani, Semicond. Sci. Technol. **12**, 141 (1997).
[44] A. Greiner, L. Reggiani, T. Kuhn, and L. Varani, Phys. Rev. Lett. **78**, 1114 (1997).
[45] M. Nedjalkov, H. Kosina, and S. Selberherr, *Proceedings of SISPAD'99*, edited by K. Taniguchi and N. Nakayama (Business Center for Academic Societies Japan, Kyoto, 1999), p. 155.
[46] R. Brunetti, P. Golinelli, M. Rudan, and L. Reggiani, J. Appl. Phys. **85**, 1572 (1999).
[47] C. Jacoboni and P. Lugli, *The Monte Carlo Method for Semiconductor Device Simulation* (Springer-Verlag, Vienna, 1989).
[48] *Monte Carlo Device Simulation: Full Band and Beyond*, edited by Karl Hess (Kluwer, Boston, 1991).
[49] M. O. Vassel, J. Math. Phys. **11**, 408 (1970).
[50] K. Kometer, G. Zandler, and P. Vogl, Phys. Rev. B **46**, 1382 (1992).
[51] M. A. Alam, M. A. Stettler, and M. S. Lundstrom, Solid-State Electron. **36**, 263 (1993).
[52] N. Goldsman, Yu.-Jen Wu, and J. Frey, J. Appl. Phys. **68**, 1075 (1990).
[53] H. M. J. Boots, Phys. Rev. B **46**, 9428 (1992).
[54] E. Starikov and P. Shiktorov, Fiz. Tekh. Poluprovodn. (S.-Peterburg) **22**, 72 (1988).
[55] C. Canali, C. Jacoboni, F. Nava, G. Ottaviani, and A. Alberigiquaranta, Phys. Rev. B **12**, 2265 (1975).
[56] M. J. Martin, T. Gonzalez, J. E. Velasquez, and D. Pardo, Semicond. Sci. Technol. **8**, 1291 (1993).
[57] M. Fischetti, IEEE Trans. Electron Devices **38**, 634 (1991).
[58] P. M. Smith, M. Inoue, and Jeffrey Frey, Appl. Phys. Lett. **37**, 797 (1980).
[59] E. Hairer and G. Wanner, *Solving Ordinary Differential Equations II, Stiff and Differential-Algebraic Problems* (Springer-Verlag, Berlin, 1991).